OAK RIDGE NATIONAL LABORATORY
operated by
UNION CARBIDE CORPORATION
NUCLEAR DIVISION
for the
U.S. ATOMIC ENERGY COMMISSION

ORNL-TM-1312,
Volume 9

DATE ISSUED: FEB 5 1971

STRUCTURAL ANALYSIS OF SHIPPING CASKS
VOL. 9. ENERGY ABSORPTION CAPABILITIES OF PLASTICALLY DEFORMED STRUTS UNDER SPECIFIED IMPACT LOADING CONDITIONS

(Thesis)

F. C. Davis

Submitted as a thesis to the Graduate Council of The University of Tennessee in partial fulfillment of the requirements for the Master of Science degree with a major in Engineering Mechanics.

ORNL TM-1312
VOL. 9

Contract No. W-7405-eng-26

General Engineering Division

STRUCTURAL ANALYSIS OF SHIPPING CASKS
VOL. 9. ENERGY ABSORPTION CAPABILITIES OF PLASTICALLY DEFORMED STRUTS UNDER SPECIFIED IMPACT LOADING CONDITIONS

F. C. Davis

The material contained herein was submitted to the Graduate Council of The University of Tennessee in partial fulfillment of the requirements for the Master of Science degree with a major in Engineering Mechanics

FEBRUARY 1971

OAK RIDGE NATIONAL LABORATORY
Oak Ridge, Tennessee
operated by
UNION CARBIDE CORPORATION
for the
U.S. ATOMIC ENERGY COMMISSION

ACKNOWLEDGMENTS

The author wishes to express his gratitude to Dr. Hui Pih of the Engineering Mechanics Department of The University of Tennessee for his advice and time spent throughout the duration of this investigation. The author is also grateful for the support of the Chemical Technology Division and the General Engineering Division of Oak Ridge National Laboratory, which is operated by Union Carbide Corporation under contract with the United States Atomic Energy Commission, and for the assistance of Messrs. J. H. Evans and W. C. T. Stoddart of the General Engineering Division during this investigation.

ABSTRACT

The purpose of this investigation was to determine the energy absorption characteristics of plastically deformed inclined struts under impact loading. This information is needed to provide a usable method by which designers and analysts of shipping casks for radioactive or fissile materials can determine the energy absorption capabilities of external longitudinal fins on cylindrical casks under specified impact conditions. A survey of technical literature related to experimental determination of the dynamic plastic behavior of struts revealed no information directly applicable to the immediate problem, especially in the impact velocity ranges desired, and an experimental program was conducted to obtain the needed data.

Mild-steel struts with rectangular cross sections were impacted by free-falling weights dropped from known heights. These struts or fin specimens were inclined at five different angles to simulate different angles of impact that fins on a shipping cask could experience under certain accident conditions. The resisting force of the deforming strut was measured and recorded as a function of time by using load cells instrumented with resistance strain gage bridges, signal conditioning equipment, an oscilloscope, and a Polaroid camera. The acceleration of the impacting weight was measured and recorded as a function of time during the latter portion of the testing program by using an accelerometer attached to the drop hammer, appropriate signal conditioning equipment, the oscilloscope, and the camera.

A digital computer program was prepared to numerically integrate the force-time and acceleration-time data recorded during the tests to obtain deformation-time data. The force-displacement relationships were then integrated to obtain values of absorbed energy with respect to deformation or time. The results for various fin specimen geometries and impact angles are presented graphically, and these curves may be used to compute the energy absorption capacity of a longitudinal fin on a shipping cask as a function of its geometry and the percentage of deformation it is expected to experience as well as the peak force to which the fin would be subjected during the impact resulting from a 30-foot free drop onto an essentially unyielding horizontal surface.

TABLE OF CONTENTS

SECTION	PAGE
1. INTRODUCTION	1
2. LITERATURE REVIEW	5
3. DEVELOPMENT OF EXPERIMENTAL PROGRAM AND APPARATUS	9
Experimental Program Philosophy	9
Experimental Equipment and Instrumentation	10
Instrument Calibration and Preliminary Tests	15
Design and Fabrication of Test Specimens	19
4. PERFORMANCE OF TESTS	23
5. DATA TRANSFORMATION AND EVALUATION	27
The Computer Program	27
Evaluation of Test Results	28
6. CONCLUSIONS AND RECOMMENDATIONS	49
Conclusions	50
Recommendations	51
LIST OF REFERENCES	55
APPENDIXES	
A. LOAD CELL CALIBRATION CURVES	57
B. DATA TRANSFORMATION COMPUTER PROGRAM	62
C. EXAMPLE PROBLEM	77
VITA	80

LIST OF FIGURES

FIGURE		PAGE
2.1.	General Configuration of Some Beams Tested Under Conditions of Gross Deformation.	6
3.1.	The Oak Ridge National Laboratory Drop Tower.	11
3.2.	Equipment Used in Impact Tests at the Oak Ridge National Laboratory Drop Tower	13
3.3.	Load Cell and Schematic Diagram of Instrumentation Used to Measure Force-Time Relationships During the Impact Tests	14
3.4.	Schematic Diagram of Instrumentation Used to Measure Acceleration-Time Relationships During the Impact Tests .	16
3.5.	Schematic Diagram of Instrumentation Used to Measure Free-Fall Velocity in the Preliminary Tests	18
3.6.	Cross Section of Cylindrical Cask With Radial Fins Impacting a Horizontal Surface.	19
3.7.	Dimensions of Fin Specimen Configurations Tested.	21
4.1.	Force-Time Photograph Taken During Impact Test of a 6-Inch-High Fin Specimen 1/2 Inch Thick With a Zero-Degree Angle of Inclination	24
4.2.	Force-Time Photograph Taken During Impact Test of a 3.5-Inch-High Fin Specimen 1/2 Inch Thick With a Zero-Degree Angle of Inclination	24

FIGURE PAGE

4.3. Force-Time and Acceleration-Time Photograph Taken During Impact Test of an 8-Inch-High Fin Specimen 1/2 Inch Thick With a 30-Degree Angle of Inclination 26

4.4. Force-Time and Acceleration-Time Photograph Taken During Impact Test of a 4-Inch-High Fin Specimen 3/8 Inch Thick With a 40-Degree Angle of Inclination 26

5.1. The Absorbed Energy Derived From Load Cell Test Data Divided by the Plastic Moment as a Function of the Percentage of Deformation Experienced by Impacted Specimens With a Zero-Degree Angle of Inclination 29

5.2. The Absorbed Energy Derived From Load Cell Test Data Divided by the Plastic Moment as a Function of the Percentage of Deformation Experienced by Impacted Specimens With a 10-Degree Angle of Inclination 30

5.3. The Absorbed Energy Derived From Load Cell Test Data Divided by the Plastic Moment as a Function of the Percentage of Deformation Experienced by Impacted Specimens With a 20-Degree Angle of Inclination 31

5.4. The Absorbed Energy Derived From Load Cell Test Data Divided by the Plastic Moment as a Function of the Percentage of Deformation Experienced by Impacted Specimens With a 30-Degree Angle of Inclination 32

FIGURE PAGE

5.5. The Absorbed Energy Derived From Load Cell Test Data Divided by the Plastic Moment as a Function of the Percentage of Deformation Experienced by Impacted Specimens With a 40-Degree Angle of Inclination 33

5.6. The Absorbed Energy Derived From Accelerometer Test Data Divided by the Plastic Moment as a Function of the Percentage of Deformation Experienced by Impacted Specimens With a 20-Degree Angle of Inclination 35

5.7. The Absorbed Energy Derived From Accelerometer Test Data Divided by the Plastic Moment as a Function of the Percentage of Deformation Experienced by Impacted Specimens With a 30-Degree Angle of Inclination 36

5.8. The Absorbed Energy Derived From Accelerometer Test Data Divided by the Plastic Moment as a Function of the Percentage of Deformation Experienced by Impacted Specimens With a 40-Degree Angle of Inclination 37

5.9. Typical Fin Specimens With Angles of Inclination of 0, 10, 20, 30, and 40 Degrees Before and After Impact. . . . 39

5.10. The Peak Force Derived From Load Cell Test Data as a Function of Specimen Height Divided by Thickness for Impacted Specimens With a Zero-Degree Angle of Inclination 42

FIGURE PAGE

5.11. The Peak Force Derived From Load Cell Test Data as a Function of Specimen Height Divided by Thickness for Impacted Specimens With a 10-Degree Angle of Inclination 43

5.12. The Peak Force Derived From Load Cell Test Data as a Function of Specimen Height Divided by Thickness for Impacted Specimens With a 20-Degree Angle of Inclination 44

5.13. The Peak Force Derived From Load Cell Test Data as a Function of Specimen Height Divided by Thickness for Impacted Specimens With a 30-Degree Angle of Inclination 45

5.14. The Peak Force Derived From Load Cell Test Data as a Function of Specimen Height Divided by Thickness for Impacted Specimens With a 40-Degree Angle of Inclination 46

A.1. Calibration Curve for the Load Cell With a Maximum Capacity of 16,000 Pounds 58

A.2. Calibration Curve for the Load Cell With a Maximum Capacity of 32,000 Pounds 59

A.3. Calibration Curve for the Load Cell With a Maximum Capacity of 120,000 Pounds. 60

A.4. Calibration Curve for the Load Cell With a Maximum Capacity of 300,000 Pounds. 61

1. INTRODUCTION

The increasing industrial and medical use of radioisotopes and the substantial increase in the number of nuclear power plants placed in operation during the past decade have caused a great increase in the quantity of radioactive materials that must be transported from one location to another. Future generations of nuclear power reactors are projected to include fast breeder reactors, thermal reactors, and pressurized-water reactors similar to units currently in operation. The amount of spent fuel from these power plants is predicted to reach possibly 4,000 tons by the year 1980. Spent fuel assemblies withdrawn from these reactors must be transported from the reactor sites to a centralized fuel reprocessing facility for reclamation of the fissionable materials. The reclaimed materials will then be used to fabricate new fuel assemblies that will be transported back to the reactor sites. Such highly radioactive materials will necessarily have to be transported in packages or shipping casks whose primary functions are the provision of shielding to protect property and persons from the emissions of the radioactive materials and the protection of these materials.

When a package containing radioactive or fissile material is shipped from one location to another, the package is subject to regulations governing its structural integrity and its shielding and heat dissipating capabilities. The governing regulations are set forth in Chapter 0529 of the United States Atomic Energy Commission Manual (1)* and in Title

---

*Numbers within parentheses in the text designate numbered references given in the List of References.

10, Part 71, of the Code of Federal Regulations (2). Conformance of the shipping package or cask with the regulations must be demonstrated by test, experimental, or analytical methods to the United States Atomic Energy Commission or the Department of Transportation or both before a license is issued authorizing the use of a cask for the shipment of specified radioactive or fissile materials.

As well as stipulating general standards and structural standards for packaging and standards for normal conditions of transport, these regulations require that the effectiveness of the shipping cask be maintained within specified limits during and after prescribed hypothetical accident conditions. The first condition of the hypothetical accident is that the shipping cask be subjected to a free drop through a distance of 30 feet onto a flat essentially unyielding horizontal surface, striking the surface in a position in which maximum damage is expected. Conformance of a shipping cask to this hypothetical accident condition could be literally demonstrated by subjecting a full-size or a reduced-size scale model of the cask to the prescribed condition. This has been done in the past, but this method of demonstrating compliance is limited because of the expense involved. The more usual practice is to show conformance by analytical means.

Many shipping casks have external fins or ribs welded to the outer shell for additional structural strength or for heat transfer purposes. An impact such as that required by the first condition of the hypothetical accident will result in gross deformation of these fins. A theoretical analysis to determine the energy absorbed by the fins during this gross deformation would be very difficult. Analyses based upon static

material properties normally result in ultraconservative design because the stress for a given strain will generally be much higher under impact conditions. Thus, a reliable method for determining the energy absorption properties of external fins on shipping casks would be of great help to the cask designer and analyst.

The investigation reported here was undertaken to determine the energy absorption characteristics of plastically deformed inclined struts under specified impact loading conditions. The first step taken in this investigation was a review of the technical literature to obtain information on prior work related to the gross deformation of struts under impact loading. None of the published results of work done in this field was directly applicable to this particular problem, and the decision was made to conduct an experimental program. An impact test program was developed, and the geometry and fabrication method for the test specimens were selected. The struts tested had various thicknesses, heights, and angles of inclination relative to the line of impact; but their length was maintained constant at 2 inches. These struts were designed to simulate sections of typical longitudinal fins on shipping casks. Force-time and acceleration-time relationships were obtained and recorded during the tests, a computer program was written to transform the test data to energy-deformation relationships, and the results were evaluated.

The results of the literature survey are presented in Section 2. Development of the experimental program, test apparatus, and specimens tested are discussed in Section 3. Performance of the actual tests is described in Section 4, and the transformation of the resulting test

data and its evaluation are discussed in Section 5. A summary of the procedures used in this experimental program, the conclusions drawn from its results, and recommendations for future work are presented in Section 6.

2. LITERATURE REVIEW

A search of published literature was conducted to find information on the gross deformation and energy absorption characteristics of struts under impact loading and to study established approaches to investigations conducted to determine these characteristics. The search revealed no published information directly applicable to the immediate problem of developing a usable and reliable method for determining the energy absorption properties of external fins on shipping casks and only a relatively small amount of information that would be of help in planning an experimental program to develop the desired method. Most of the published results of studies dealt with impact loading and impulse loading of beams to produce pure bending or of columns under pure compression. Impact loading of a radial fin on a shipping cask involves combined compressive and bending loads, and this makes the problem much more difficult.

A study conducted by Abrahamson and Goodier (3) dealt with the flexural buckling of rods as these rods, traveling in an axial direction, impacted a flat steel surface. These investigators developed a simple theoretical model in which buckling is treated as a pertubation of the motion associated with axial compression, and linear strain hardening corresponding to a constant strain-hardening modulus is assumed. The rod is assumed to buckle under uniform axial strain. This model predicted the time scale and wavelengths observed during the tests reasonably well. The results indicated a linear relationship between the

decrease in the length of a rod specimen and the ratio of kinetic energy of the specimen to the elastic strain energy it can absorb.

An account is given by Rawlings (4) of his investigation of the energy absorption of dynamically and statically loaded beams undergoing gross deformation. The general configuration of some of these beams is illustrated in Figure 2.1. Beam configurations with three different included angles were tested; these angles were 60, 90, and 120 degrees. The force values measured during dynamic loading averaged approximately 12 percent more than the values measured during static loading. This is lower than might have been expected, and Rawlings concluded that the severe degree of cold working in the manufacture of the material and fabrication of the specimens reduced the strain rate sensitivity considerably.

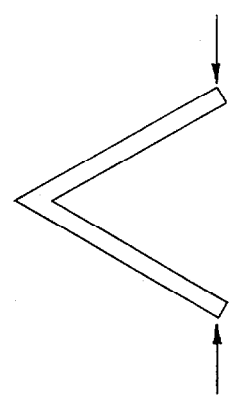

Figure 2.1. General Configuration of Some Beams Tested Under Conditions of Gross Deformation.

Work reported by Parkes (5) involved analytical and experimental studies of the plastic deformation of mild-steel cantilever beam specimens struck transversely at their tips. The experiments involved both

high-velocity (970 to 1,580 feet per second) and low-velocity (6.4 to 18 feet per second) strikers impacting the tips of mild-steel cantilevers. The cantilevers impacted had a constant cross section of 1/4 inch by 1/4 inch, but their length varied from 2 to 12 inches. The results of these experiments showed that a cantilever struck by a heavy striker with a low velocity will remain straight, deforming through an angle at the root that is independent of the length. This is similar to the type of failure expected in the quasi-static mode. The results also showed that a cantilever struck by a light striker with a high velocity will suffer a local deformation near its tip that is independent of the length and a rotation at its root that is inversely proportional to the length.

The analysis based on the concept of an ideal rigid-plastic material presented by Parkes (5) satisfactorily predicted the deformation of sections of mild steel cantilevers that were remote from the point of impact. For comparatively slow impacts, use in the analysis of a dynamic plastic moment 50 percent greater than the static plastic moment gave satisfactory agreement with the experimental results. The analysis predicted qualitatively the occurrence and behavior of the local deformation at the tip of the impacted cantilevers, but the quantitative agreement between the analytical prediction of the shape of this deformation and the high-velocity test results was poor. Parkes concluded that prediction of local damage is dependent upon an accurate definition of the conditions of striking.

Experimental tests of cantilever beams with tip masses under both impact and impulsive loadings were conducted by Bodner and Symonds (6) to evaluate the assumptions of dynamic rigid-plastic theory. These

investigators reported that the results of their tests pointed to a strain rate effect as the principal cause of discrepancy between experimental results and simple rigid-plastic theory.

However, the geometrical effects caused by large deformations were neglected in the formulation of the problem presented by Parkes (5) and by Bodner and Symonds (6). This is equivalent to the assumption that the displacements are infinitesimally small, but rigid, ideally plastic theory is applicable only if the plastic strains are much larger than the elastic strains. The results of work performed by Ting (7) show that neglect of geometry changes caused by large deformations is also responsible for part of the discrepancies between experimental results and simple rigid-plastic theory. The analytical studies performed by Ting indicate that approximately one-half of these discrepancies, a maximum of 14 percent, reported by Parkes (5) are the result of geometrical changes in the test specimens caused by large deformations. It is generally believed that the remaining discrepancies are primarily the result of strain rate effects.

Because of the review of this report published by Ting (7), the energy absorption characteristics of a plastically deformed strut or shipping cask fin are considered in this investigation to be a linear function of the length of the fin along the cask. That is, 20 inches of a fin along the length of a shipping cask will absorb 20 times the energy that 1 inch of the same fin will absorb.

3. DEVELOPMENT OF EXPERIMENTAL PROGRAM AND APPARATUS

The literature review revealed no results that would enable the designer of a shipping cask to determine the energy absorption capabilities of external longitudinal fins undergoing gross deformation. Therefore, the decision was made to develop the needed information by experimental methods. The philosophy for the experimental program was developed, the experimental equipment and instrumentation were selected, the instruments were calibrated, and the test specimens were designed and fabricated.

3.1 Experimental Program Philosophy

The general approach that was adopted for the experimental program involved dropping a hammer of known weight from a predetermined height onto a specimen and recording the force-time relationship experienced by the specimen throughout the duration of the resulting impact. Force with respect to time can be converted to acceleration with respect to time by Newton's Second Law of Motion. This acceleration-time relationship can be converted to a velocity-time relationship by using the following equation.

$$v_t = v_o - \int_{t=o}^{t=t} a \, dt, \tag{3.1}$$

where

v_t = velocity at a point in time,

v_o = initial velocity at time equal zero,

t = time, and

a = acceleration.

Similarly, the velocity-time relationship can be used to determine the deformation-time relationship by using the expression

$$X_t = \int_{t=o}^{t=t} v_t \, dt = \int_{t=o}^{t=t} v_o \, dt - \int_{t=o}^{t=t}\int_{t=o}^{t=t} a \, dt \, , \qquad (3.2)$$

where X_t = the displacement at a point in time. Knowing the force-time and deformation-time relationships, the energy absorbed can be calculated from the expression

$$U = \int_{o}^{X} P \, dx \, , \qquad (3.3)$$

where

U = energy absorbed for a specific amount of deformation,

X = deformation, and

P = applied force.

At the end of the impact duration, at which time the velocity has become zero, the calculated absorbed energy should be equal to the kinetic energy of the impacting hammer at time equal zero. This gives a time at which the experimental data can be verified.

3.2 Experimental Equipment and Instrumentation

The impact tests were conducted at the Oak Ridge National Laboratory Drop Tower shown in Figure 3.1. This structural steel tower is 40 feet high and its drop base is comprised of a surface of armor plate embedded in steel-reinforced concrete. Two 3-by-3-inch angles

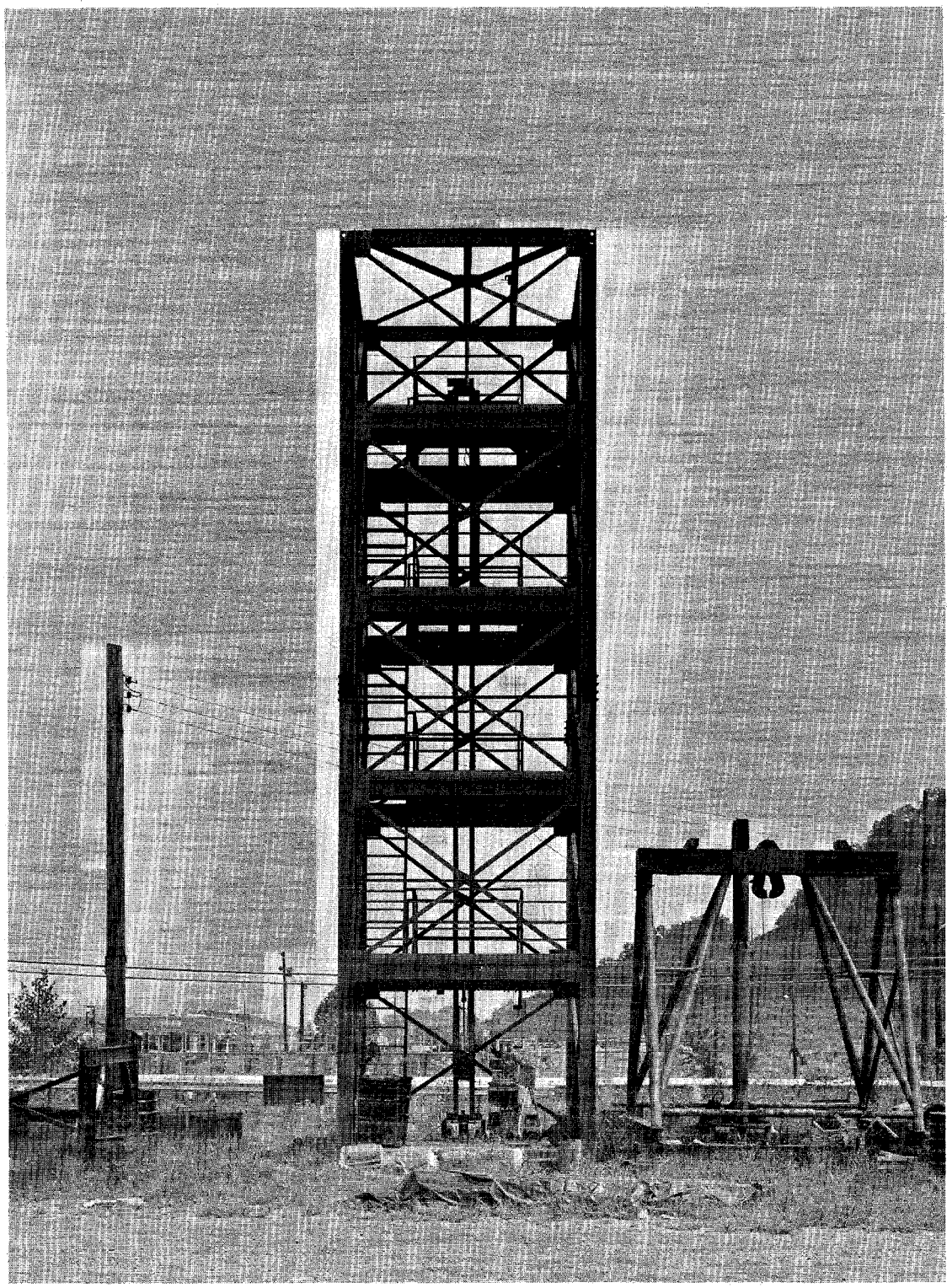

Figure 3.1. The Oak Ridge National Laboratory Drop Tower.

3/16 inch thick were attached to the tower vertically to guide the impact hammer during its free fall. The basic structure of this hammer originally weighed 94 pounds. However, the addition of some bracing became necessary during the performance of the tests, and the weight of the hammer was increased to 99 pounds. This basic hammer weight could be increased in 21-pound increments by the addition of steel blocks to the hammer, and a maximum weight of approximately 500 pounds could be obtained. The guide rails, weights, impact hammer, and the other equipment used in the impact tests are shown in Figure 3.2.

Three load cells were designed to provide different ranges of sensitivity from 0 to 300,000 pounds necessary to cover the fin geometries of interest. The three cells were cylinders 8 inches long with an outside diameter of 6 inches. The inside diameters of these cells were 5.9 inches, 5.5 inches, and 4.5 inches. The load cell with the smallest maximum capacity (16,000 pounds) was damaged during the course of the tests, and a replacement cell was made that had an inside diameter of 5.8 inches. These load cells were fabricated of mild steel. Bonded resistance strain gages were secured to the periphery of the load cells with epoxy resin and wired into a full Wheatstone bridge arrangement, as illustrated in Figure 3.3. This arrangement afforded a 5.2 amplification of the output signal, as compared with the output of a single strain gage.

A 12-volt automotive battery was used as a power source for the Wheatstone bridge, which was connected to a bridge balancing unit. The output of the bridge was fed to one channel of a dual-beam Tektronix Type 565 oscilloscope with a Type 3A3 dual trace differential amplifier.

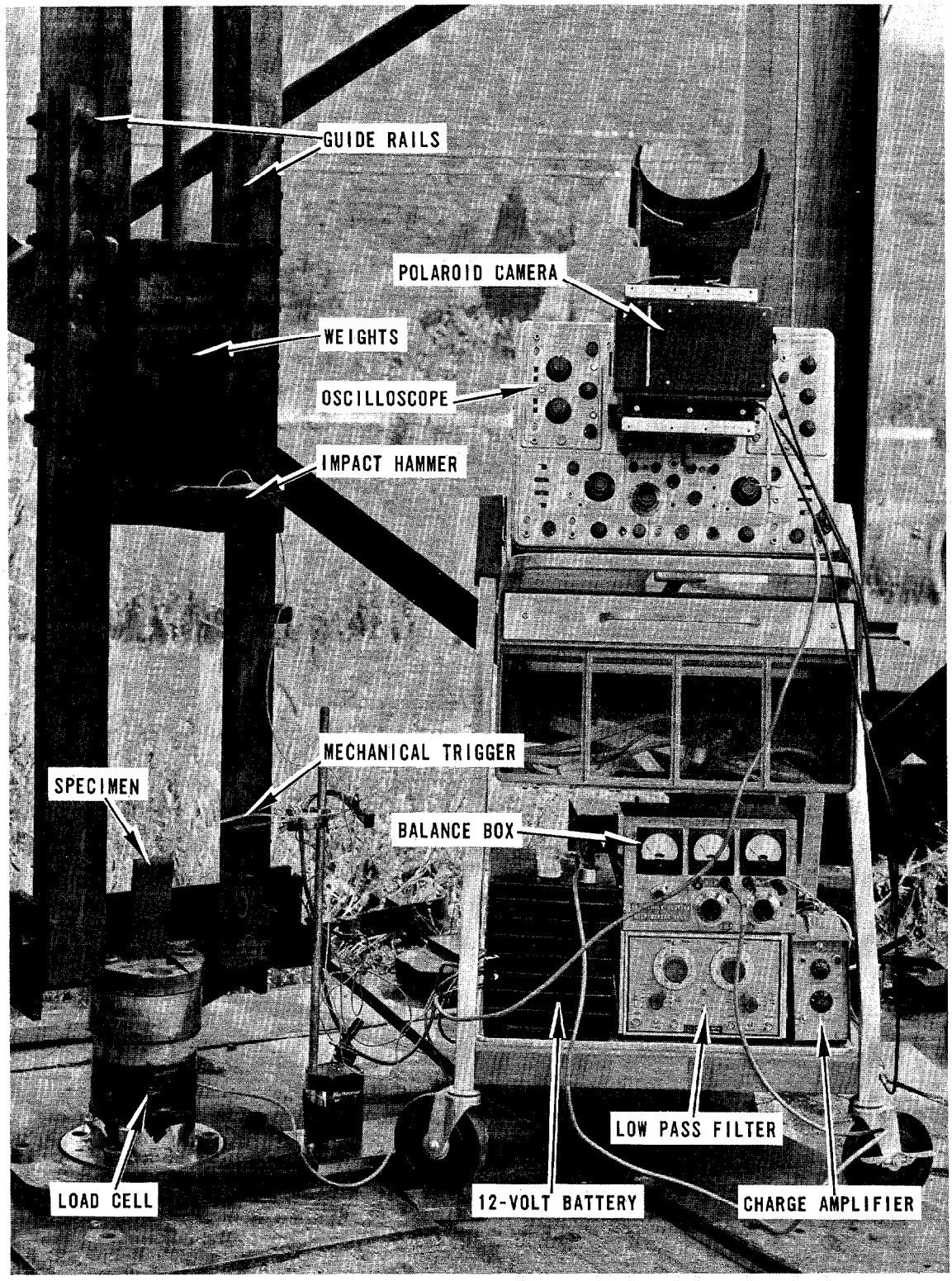

Figure 3.2. Equipment Used in Impact Tests at the Oak Ridge National Laboratory Drop Tower.

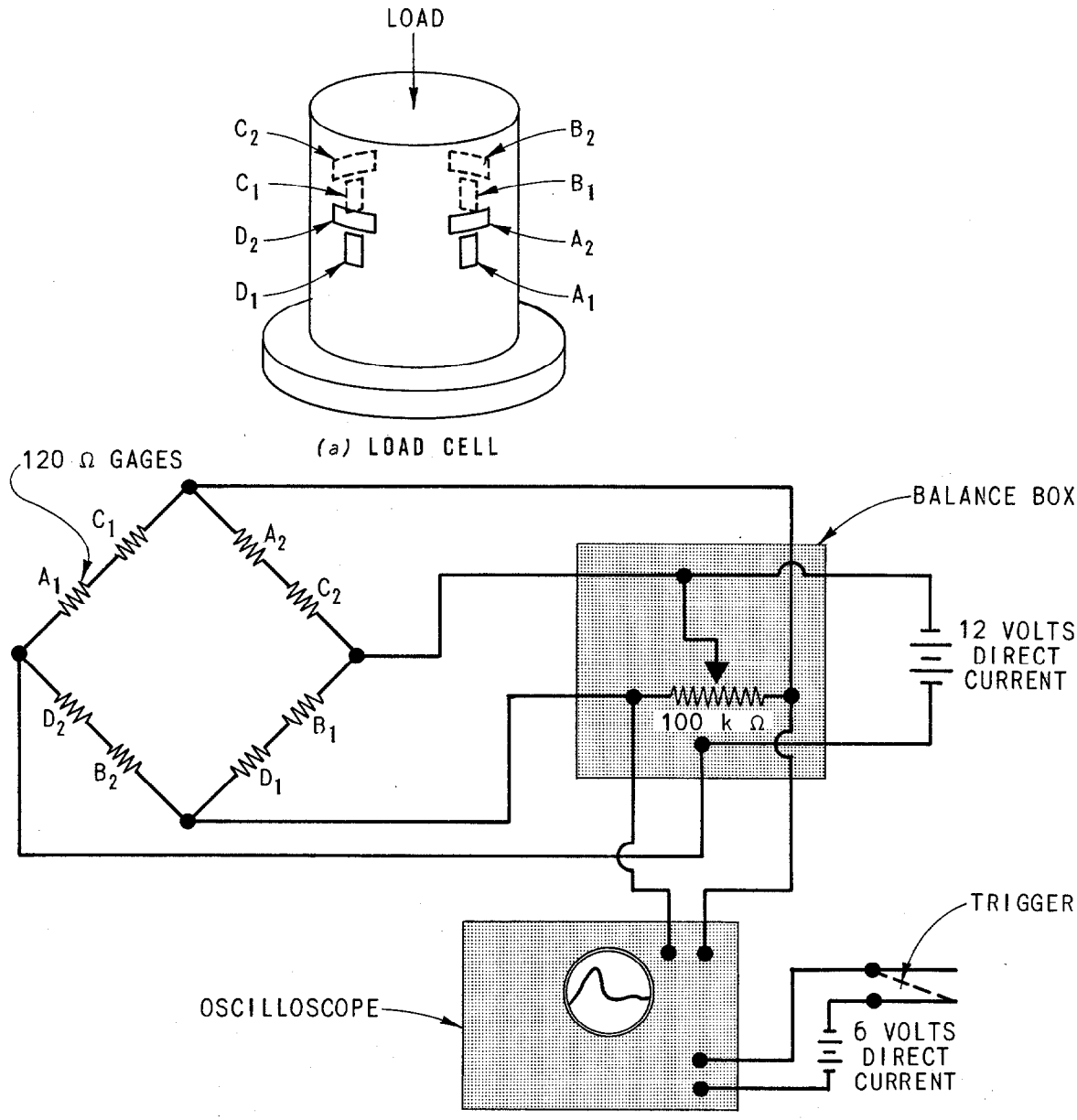

Figure 3.3. Load Cell and Schematic Diagram of Instrumentation Used to Measure Force-Time Relationships During the Impact Tests.

A battery powered mechanical trigger was used to initiate the single sweep on the oscilloscope, and the trace was recorded on film by using a Polaroid Land camera attachment on the oscilloscope.

The equipment described was used throughout all of the tests to obtain impact force-time relationships. During the latter half of these tests, acceleration-time relationships were also obtained by attaching a piezoelectric accelerometer to the hammer and feeding its output signal through a charge amplifier and a low-pass filter to the second channel of the oscilloscope. With the incorporation of this instrumentation, as illustrated in Figure 3.4, a force-time relationship and an acceleration-time relationship were recorded simultaneously for each impact. The low-pass filter was required because the high frequencies experienced during the impacts caused the signal from the accelerometer to be completely obscured by the high-frequency noise.

3.3 Instrument Calibration and Preliminary Tests

The load cells were calibrated by using a Baldwin 120,000-pound hydraulic compression testing machine. Two of the original three load cells were loaded to capacity (16,000 pounds and 120,000 pounds) during calibration, while the third cell with a 300,000-pound capacity was loaded only to the capacity of the testing machine. Based on the linearity of the calibrated portion, it was assumed that the response of this large cell continued to be linear throughout its range. The replacement cell with a capacity of 32,000 pounds was also loaded to its capacity and calibrated before being placed in service. The calibration curves for these load cells are given in Appendix A.

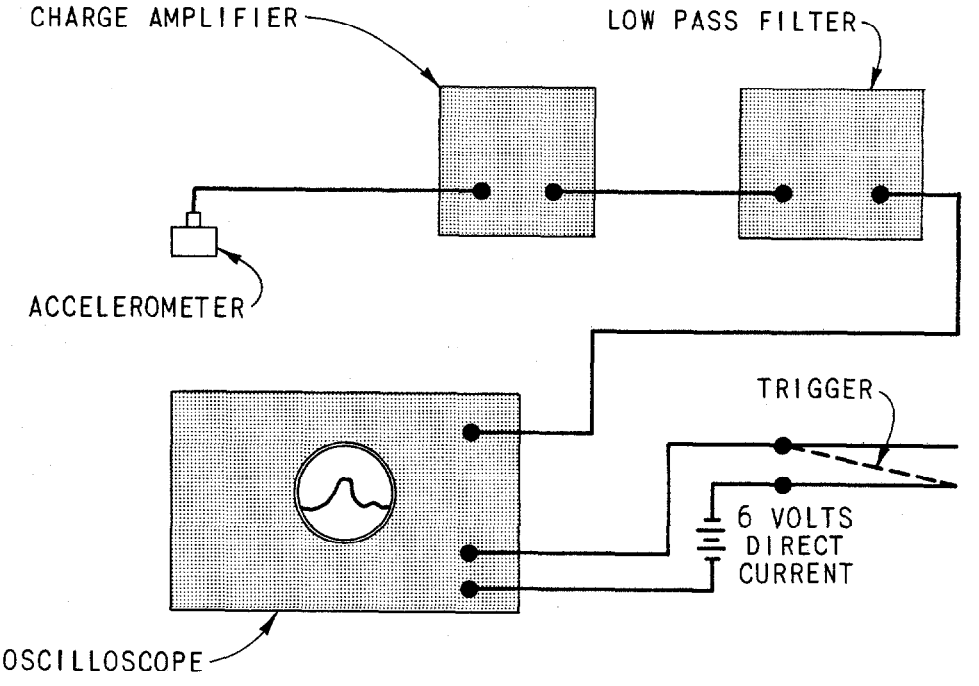

Figure 3.4. Schematic Diagram of Instrumentation Used to Measure Acceleration-Time Relationships During the Impact Tests.

Preliminary tests were performed to determine the significance of the frictional force developed between the guides and the hammer during the free fall of the hammer. A schematic diagram of the test setup is illustrated in Figure 3.5. Three fine wires were tautly fastened in the path of the falling hammer, and each of these wires had an electrical potential of 6 volts applied to it. Breaking of the first wire by the falling hammer provided the signal to initiate the sweep on the oscilloscope. Breaking of the second wire and the third wire by the falling hammer provided signals evidenced on the oscilloscope. With the distance between the second and third wires known (10 inches) and the time required to travel that distance recorded by the oscilloscope, the average velocity of the hammer traveling that distance was calculated from the expression

$$v = \frac{x}{t}, \tag{3.4}$$

where

v = velocity in feet per second,

x = distance in feet, and

t = time in seconds.

During these preliminary tests, the hammer was released from heights of 10, 20, and 30 feet. The distance between the second and third wires was held constant at 10 inches. The values of velocity determined in this manner were compared with theoretical values calculated by using the expression

$$v = (2gh)^{1/2}, \tag{3.5}$$

where

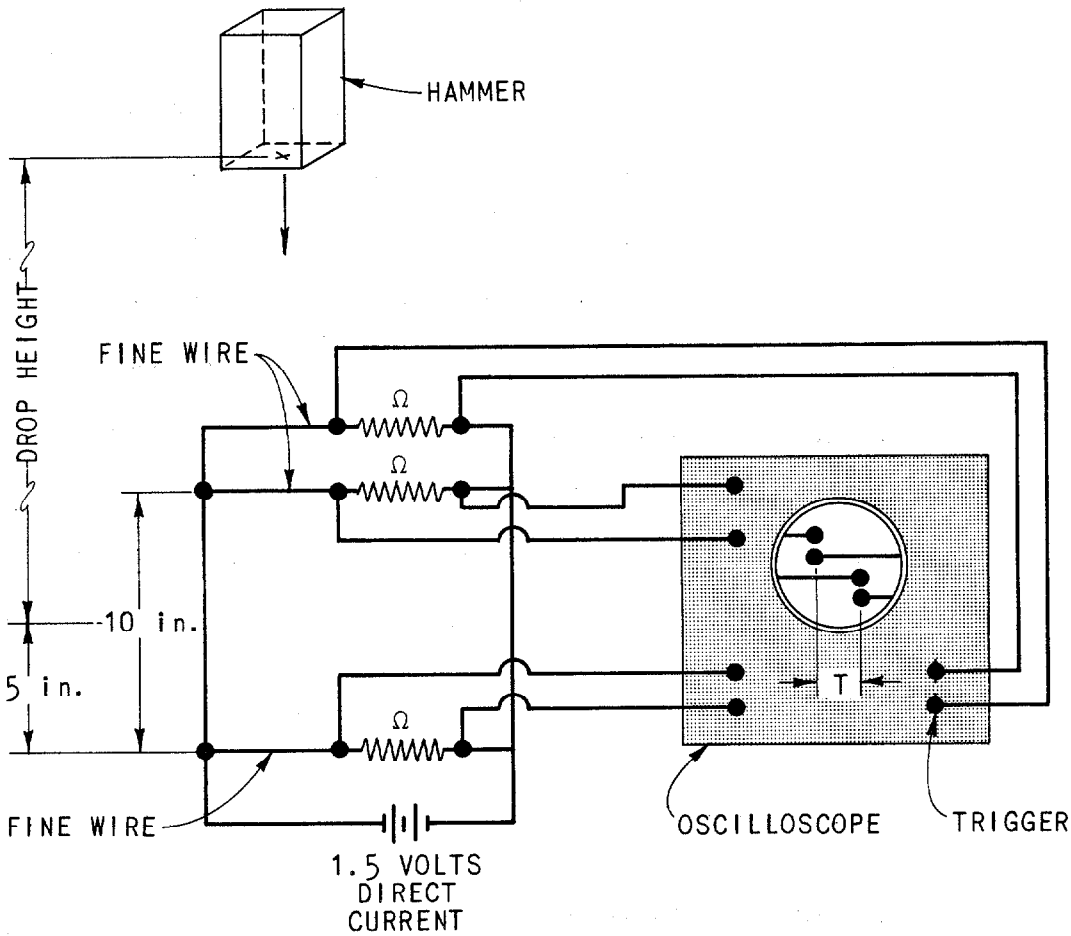

Figure 3.5. Schematic Diagram of Instrumentation Used to Measure Free-Fall Velocity in the Preliminary Tests.

g = gravitational constant of 32.2 feet per second, and

h = height from which the hammer was dropped or the vertical distance through which the hammer fell in feet.

The greatest deviation between the free-fall velocities calculated by using Equation 3.4 and the theoretical velocities calculated by using Equation 3.5 was less than 2 percent. This value was considered relatively small, and theoretical velocity values were used in the calculations made in this investigation.

3.4 Design and Fabrication of Test Specimens

Consider the cross section of a cylindrical cask with longitudinal fins along its axis impacting a horizontal level surface, as is illustrated in Figure 3.6. It is obvious that only one fin may have an angle of inclination of zero degrees, while the angle of inclination of adjacent fins will vary according to the position of the fins around the circumference of the cask. The decision was made to test fin specimens at five different angles of inclination: 0, 10, 20, 30, and 40 degrees.

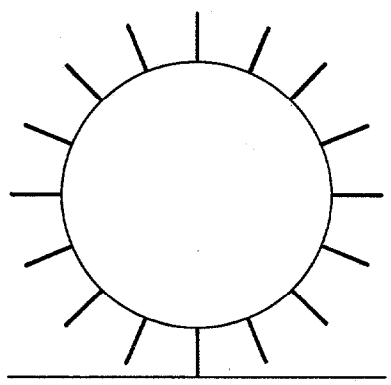

Figure 3.6. Cross Section of Cylindrical Cask With Radial Fins Impacting a Horizontal Surface.

Angles of inclination greater than 40 degrees are not feasible because under normal circumstances, the body of the cask will have contacted the impact surface before angles of inclination greater than 40 degrees can be realized.

Many designs for shipping casks specify hot-rolled mild steel as the material used for the outer shell of the cask. The American Society for Testing and Materials Specification ASTM A 285, Grade C, Fire Box Quality, defines a common material of this type that was selected for the test specimens. This material has a yield strength of 30,000 pounds per square inch.

As a result of the findings presented by Ting (7) that were discussed in Section 2, the energy absorption characteristics of longitudinal fins on shipping casks are considered a linear function of the length of the fin in this investigation. Thus, the decision was made to fabricate all of the test specimens with the same length. This decision permitted the use of a common set of test fixtures and made transformation of the test data somewhat easier.

Five specimens of each configuration illustrated in Figure 3.7 were fabricated. The weight capacity of the hammer hoist dictated the length of a specimen that could be accommodated and deformed significantly in the impact tests. After consideration was given to the more rigid specimens, a length of 2 inches was selected for all of the specimens that were fabricated. As illustrated in Figure 3.7, the base of the specimen is perpendicular to the fin only for those specimens whose angle of inclination is zero degrees. The non-perpendicularity of the other specimens does not simulate the actual configuration of a fin on a

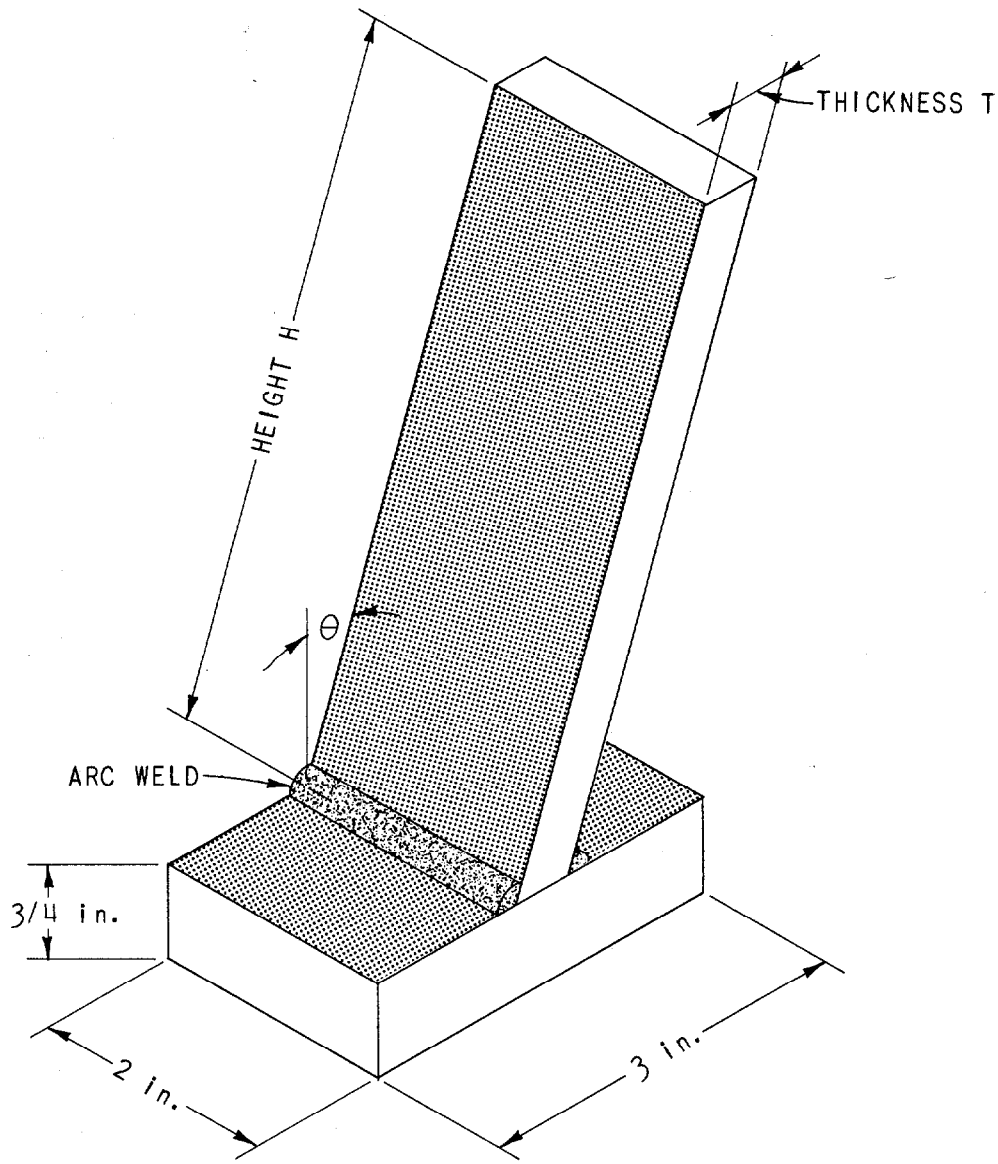

T (in.)	θ																				
	0°					10°				20°				30°				40°			
	H (in.)																				
	3½	4	6	8	9	4	6	8	10	4	6	8	10	4	6	8	10	4	6	8	10
1/4		X	X				X	X	X		X	X	X		X	X	X		X	X	X
3/8						X	X	X	X	X	X	X	X	X	X	X		X	X	X	X
1/2	X		X	X		X	X	X	X	X	X	X	X	X	X	X	X	X	X	X	X
5/8							X	X	X	X	X	X	X	X	X	X		X	X	X	X
3/4			X		X	X	X	X	X	X	X	X	X	X	X		X	X	X	X	X

Figure 3.7. Dimensions of Fin Specimen Configurations Tested.

shipping cask, but this concession was made for the sake of simplicity in the test fixtures. It was felt that this concession would not materially affect the experimental results.

The fin specimens were fabricated in a manner intended to produce five identical specimens of each size. Two plates 12 inches long of the appropriate thickness and width were welded together at the desired angle. One inch was cut off of each end of the weldment to eliminate possible defects in the areas where the weld beads were initiated and terminated. The remaining 10-inch-long weldment was then cut into five 2-inch-long sections to provide the five identical test specimens of that particular configuration.

4. PERFORMANCE OF TESTS

Impact tests were conducted on 275 specimens of shipping cask fins. In each test, a fin specimen of the desired geometry was securely clamped to the top of the load cell and the appropriate sweep rate and vertical scale were set on the oscilloscope. These settings were a function of the drop height, weight dropped, specimen geometry, and sensitivity of the load cell. The mechanical trigger was set a small distance above the top of the fin specimen. This distance was dependent upon the sweep rate setting of the oscilloscope. The distance decreased as the sweep rate was increased.

The hammer with an appropriate amount of added weight was raised to the desired drop height. The oscilloscope screen illumination was turned to its maximum value and the screen grid was photographed. The illumination was then turned off, the camera was set for time exposure, and the hammer was released. The free-falling hammer closed the contacts on the mechanical trigger, initiating a single sweep on the oscilloscope. Impact of the hammer on the fin specimen transmitted a force to the load cell. This force caused the strain gage bridge associated with the load cell to produce an output voltage proportional to the applied force. The voltage, which changed rapidly with time, was displayed on the oscilloscope screen and recorded by the scope camera. Typical impact force-time photographs are shown in Figures 4.1 and 4.2.

After 157 fin specimens had been impact tested, the decision was made to measure and record the acceleration-time relationships of the hammer during the tests because some ringing, which caused difficulties,

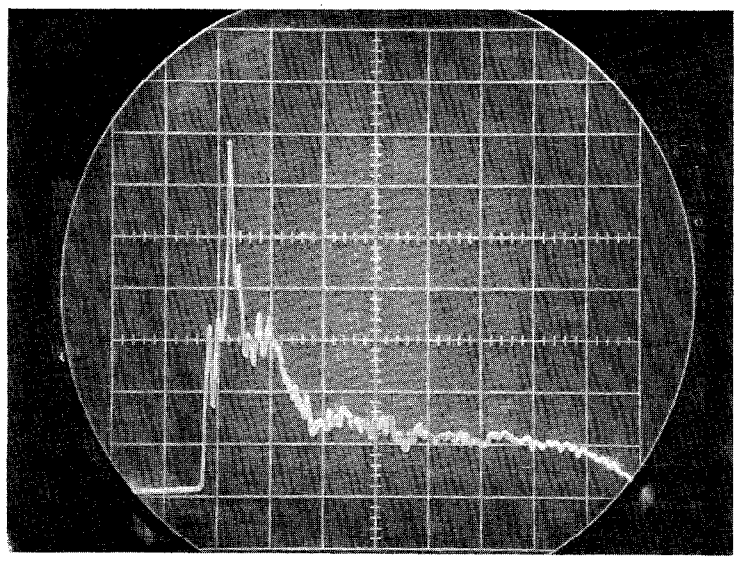

Force (20,500 lb./cm.)

Time (1 msec./cm.)

Figure 4.1. Force-Time Photograph Taken During Impact Test of a 6-Inch-High Fin Specimen 1/2 Inch Thick With a Zero-Degree Angle of Inclination.

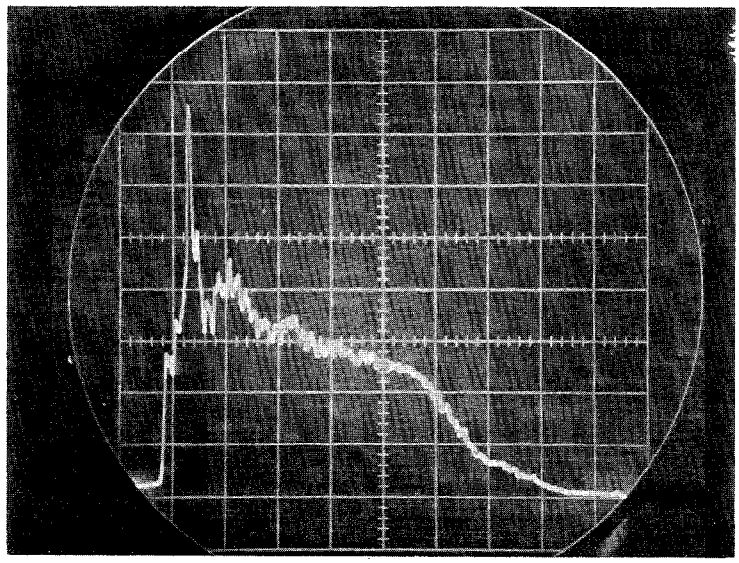

Force (20,500 lb./cm.)

Time (1 msec./cm.)

Figure 4.2. Force-Time Photograph Taken During Impact Test of a 3.5-Inch-High Fin Specimen 1/2 Inch Thick With a Zero-Degree Angle of Inclination.

had appeared in the load cell signal. An accelerometer was attached to the hammer and its output signal was transmitted to the oscilloscope through a charge amplifier and low-pass filter, as described in Subsection 3.2. Thus, the impact force-time relationship and the acceleration-time relationship for each of the remaining 118 fin specimens tested were recorded simultaneously. Typical photographs of these oscilloscope recordings are shown in Figures 4.3 and 4.4.

The geometry of the fin specimen tested, hammer weight, load cell sensitivity, and the oscilloscope settings were recorded for each impact test conducted. Each impacted specimen was removed from the load cell, identified by number, and its deformed height was measured and recorded as a basis for determination of permanent deformation. Each impact data photograph was removed from the oscilloscope camera and numbered appropriately. From the trace or traces on each photograph, coordinates of points along the curves were read, recorded, and converted to force or acceleration values as a function of time by applying the instrumentation settings and calibration values. The acceleration-time data recorded in this manner were analyzed by applying the methods discussed in Subsection 3.1 that were used to analyze the force-time data except that the force-to-acceleration computation was not required. The results obtained should be theoretically identical to those obtained by using the force-time data.

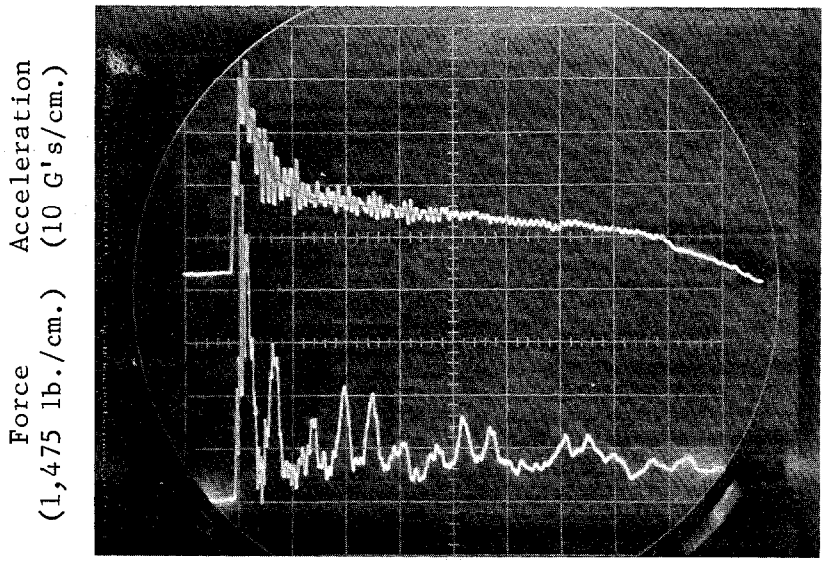

Figure 4.3. Force-Time and Acceleration-Time Photograph Taken During Impact Test of an 8-Inch-High Fin Specimen 1/2 Inch Thick With a 30-Degree Angle of Inclination.

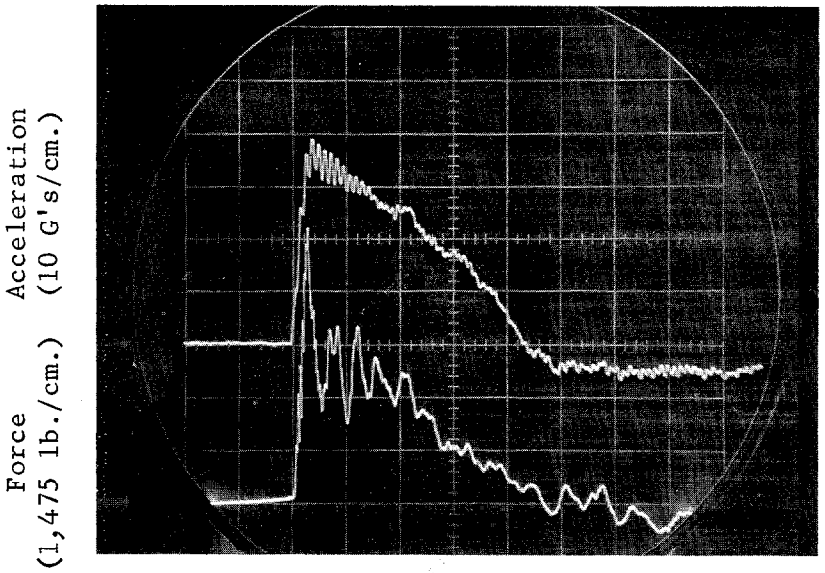

Figure 4.4. Force-Time and Acceleration-Time Photograph Taken During Impact Test of a 4-Inch-High Fin Specimen 3/8 Inch Thick With a 40-Degree Angle of Inclination.

5. DATA TRANSFORMATION AND EVALUATION

The force-time and acceleration-time data recorded during the impact tests of the fin specimens were transformed into absorbed energy-deformation data by means of a computer program prepared for this purpose. The numerical data were used as input for a computer plotting program to provide a graphical representation of the transformed test data, which were then evaluated.

5.1 The Computer Program

A Fortran program applicable to the IBM 360 computer at Oak Ridge National Laboratory was prepared to transform the force-time and acceleration-time data obtained manually from the oscilloscope photographs into absorbed energy and deformation data. This data transformation computer program listing is presented in Appendix B along with the output data for the first ten specimens that were tested.

The values of force or acceleration and the corresponding time obtained from the photographs made during each impact test were transferred to IBM data cards as were the test parameters or variables, which included the drop height, weight of hammer dropped, initial height, thickness, and angle of inclination of the specimen, and the final measured deformed height of the specimen. These cards were inserted in the computer for performance of the necessary data transformation calculations. The computational steps in the computer program listing are explained by comment cards that were inserted in appropriate locations. The computer output included a printed copy of the final computational

results and a deck of IBM cards that served as input data cards for an existing computer plotting program. The output of this plotting program is presented and discussed in Subsection 5.2.

5.2 Evaluation of Test Results

The output of the computer plotting program generated after transformation of the data obtained during the impact tests is presented graphically. The sets of curves shown in Figures 5.1 through 5.5 were derived from the force-time data obtained from the load cells during the impact tests, and the heights (H) of the specimens tested are given for their respective curves. These curves are plots of the absorbed energy divided by the plastic moment of each specimen tested versus the vertical deformation of the specimen multiplied by 100 and divided by the original height of the specimen. This abscissa dimension is essentially the percentage of total deformation possible. The plastic moment values used were calculated from the expression

$$M_p = \sigma_y\left(\frac{bt^2}{4}\right) , \tag{5.1}$$

where

M_p = static plastic moment of specimen,

σ_y = yield stress of specimen material = 30,000 pounds per square inch,

b = length of specimen = 2 inches, and

t = thickness of specimen in inches.

Therefore, the static plastic moment

$$M_p = 15{,}000t^2 \text{ inch-pounds} . \tag{5.2}$$

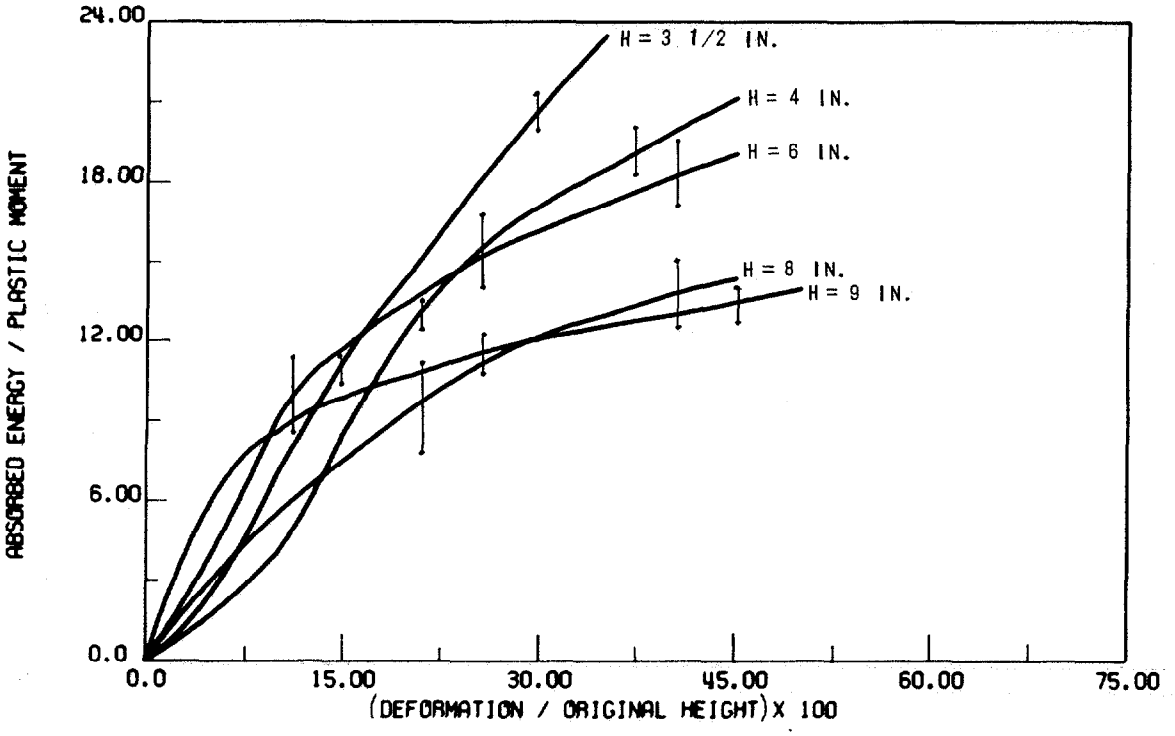

Figure 5.1. The Absorbed Energy Derived From Load Cell Test Data Divided by the Plastic Moment as a Function of the Percentage of Deformation Experienced by Impacted Specimens With a Zero-Degree Angle of Inclination.

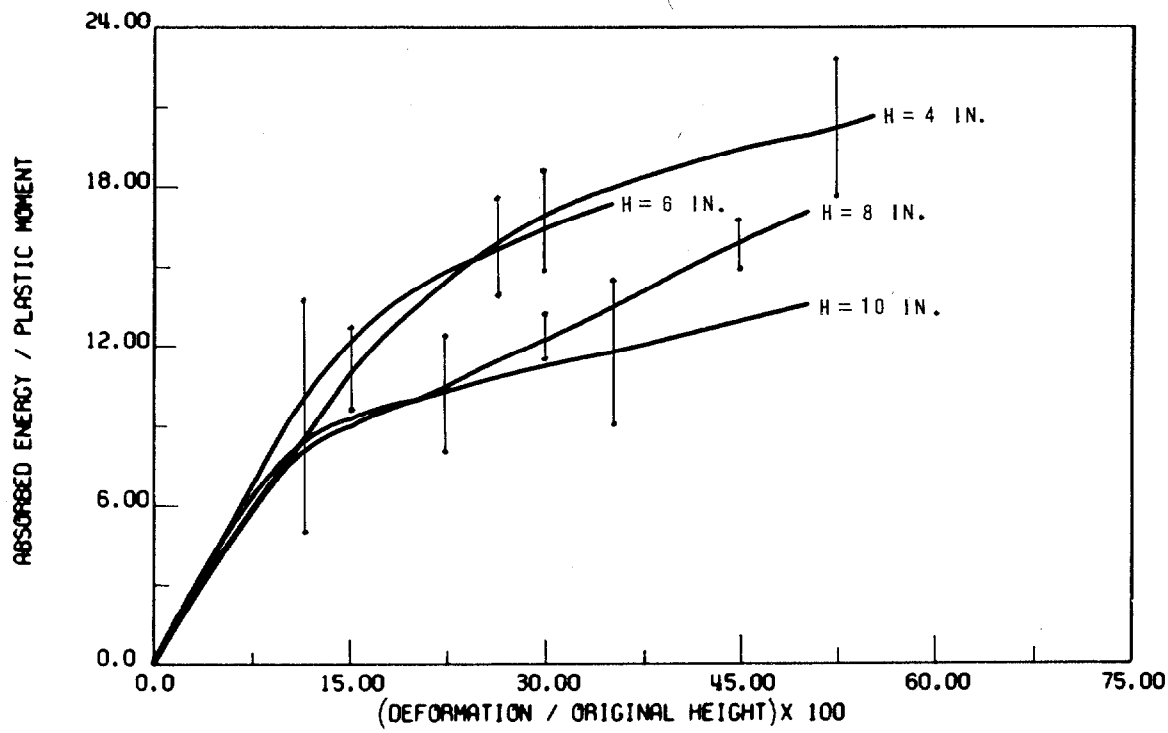

Figure 5.2. The Absorbed Energy Derived From Load Cell Test Data Divided by the Plastic Moment as a Function of the Percentage of Deformation Experienced by Impacted Specimens With a 10-Degree Angle of Inclination.

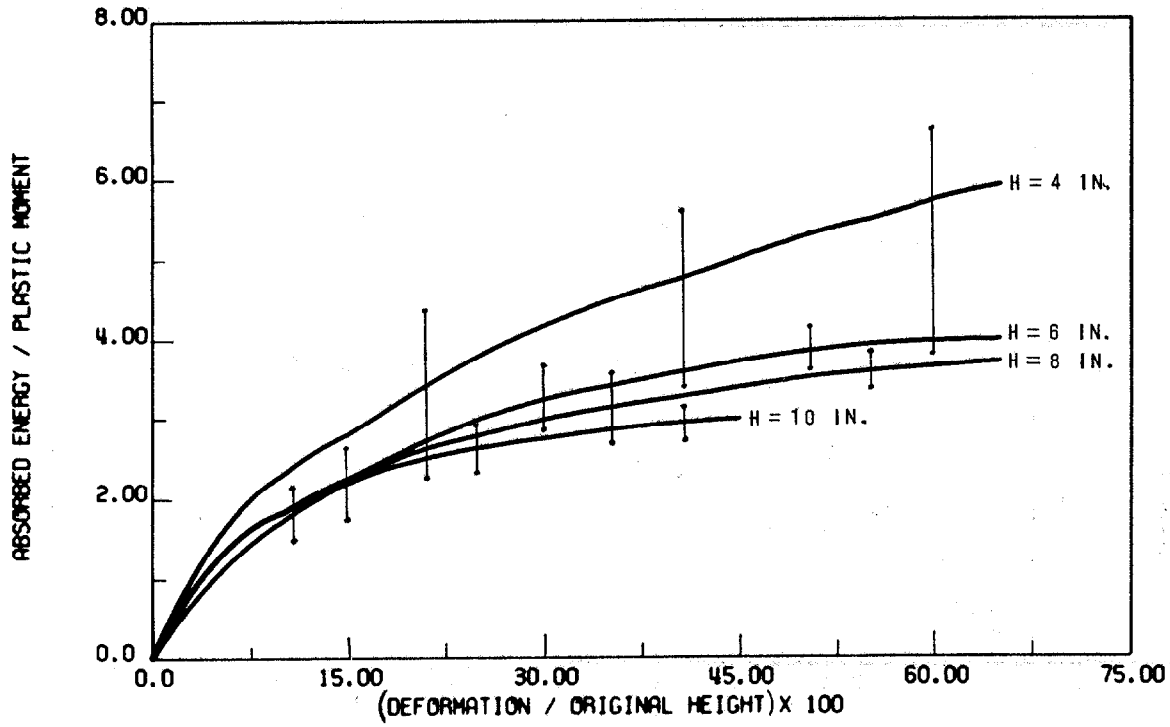

Figure 5.3. The Absorbed Energy Derived From Load Cell Test Data Divided by the Plastic Moment as a Function of the Percentage of Deformation Experienced by Impacted Specimens With a 20-Degree Angle of Inclination.

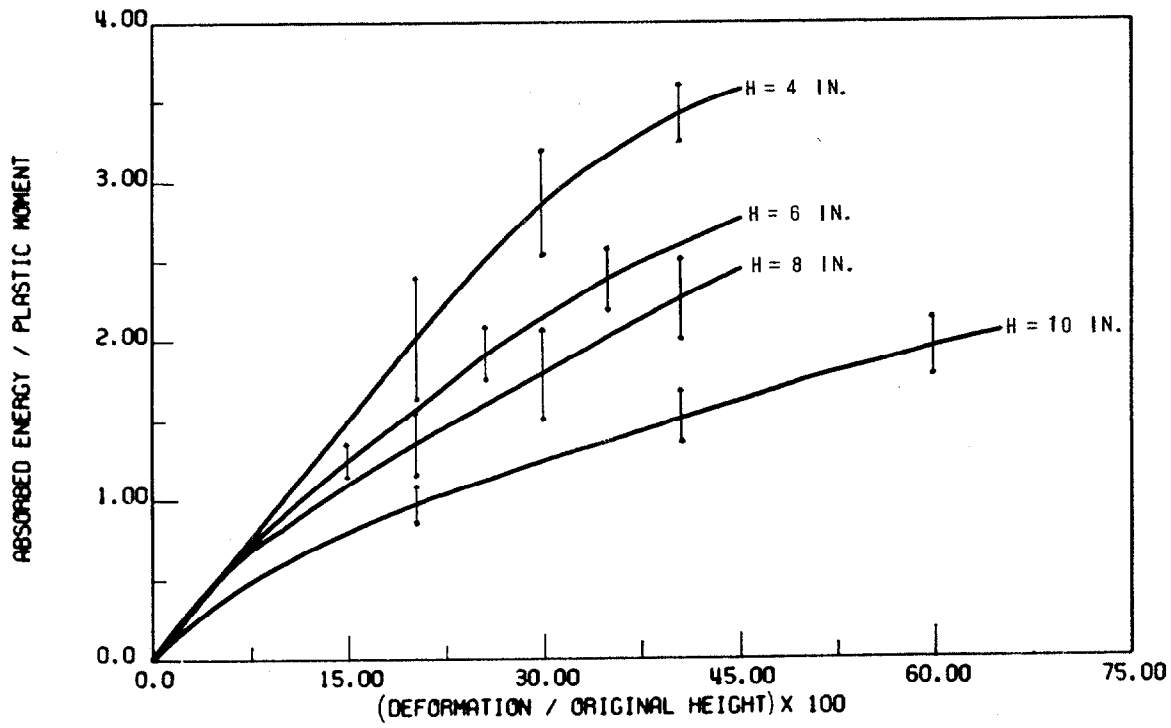

Figure 5.4. The Absorbed Energy Derived From Load Cell Test Data Divided by the Plastic Moment as a Function of the Percentage of Deformation Experienced by Impacted Specimens With a 30-Degree Angle of Inclination.

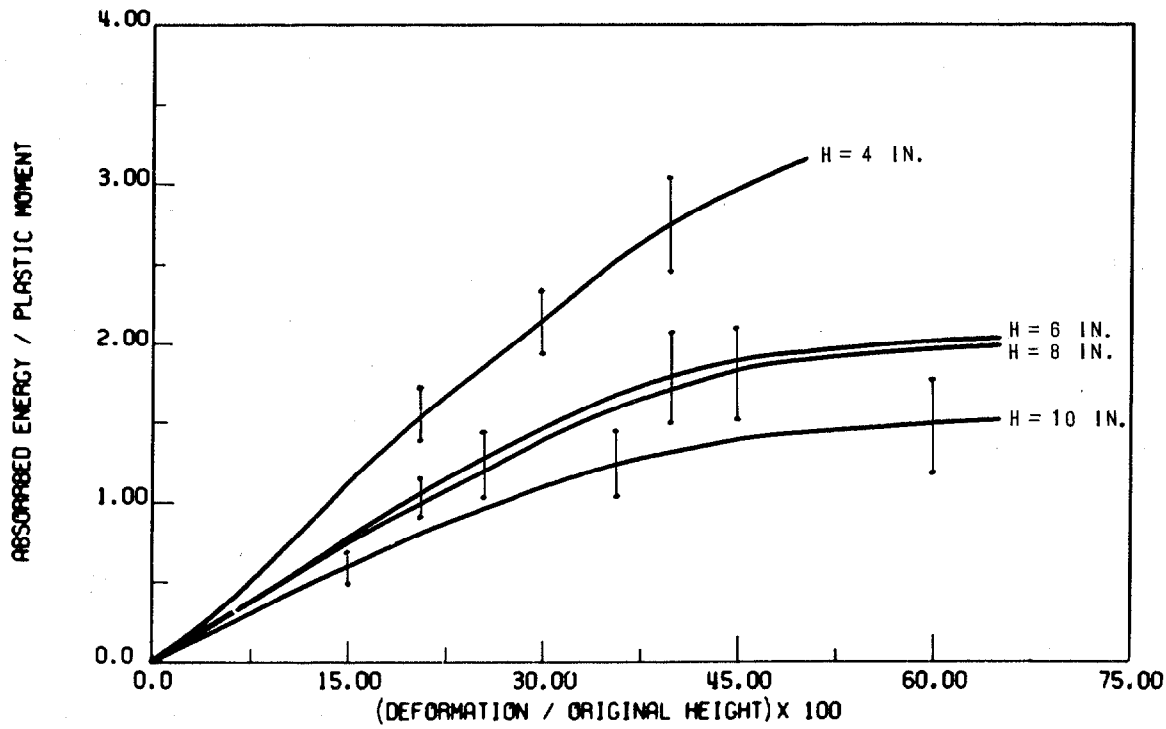

Figure 5.5. The Absorbed Energy Derived From Load Cell Test Data Divided by the Plastic Moment as a Function of the Percentage of Deformation Experienced by Impacted Specimens With a 40-Degree Angle of Inclination.

The sets of curves shown in Figures 5.6 through 5.8 were derived from the acceleration-time data obtained from the accelerometer during the impact tests. These curves are also plots of the absorbed energy divided by the plastic moment of each specimen tested versus the percentage of deformation experienced by the impacted specimen. The curves derived from the accelerometer data and those derived from the load cell data should theoretically be identical. However, careful analysis of these curves indicates that those derived from the accelerometer data show approximately 10 percent less energy absorption than those derived from the load cell data. Although not large, this discrepancy remained fairly constant, and it may be the result of a calibration error. The accelerometer was not calibrated by using the instrumentation used during performance of the tests. The calibration data received from the manufacturer were used in the analysis.

There is a vast difference between the energy absorption capabilities of the stiff (angles of inclination of 0 and 10 degrees) specimens and the less stiff (angles of inclination of 20, 30, and 40 degrees) specimens. The reason for this vast difference is that all of the specimens with zero-degree angles of inclination and most of the specimens with 10-degree angles of inclination failed in a double-hinge mode similar to the buckling type of failure expected of a column restrained at one end, whereas most of the specimens with 20-degree angles of inclination and all of the specimens with 30- and 40-degree angles of inclination failed in a single-hinge mode. Six of the 61 specimens with 10-degree angles of inclination failed in a single-hinge mode, while 12 of the 79 specimens with 20-degree angles of inclination failed in a

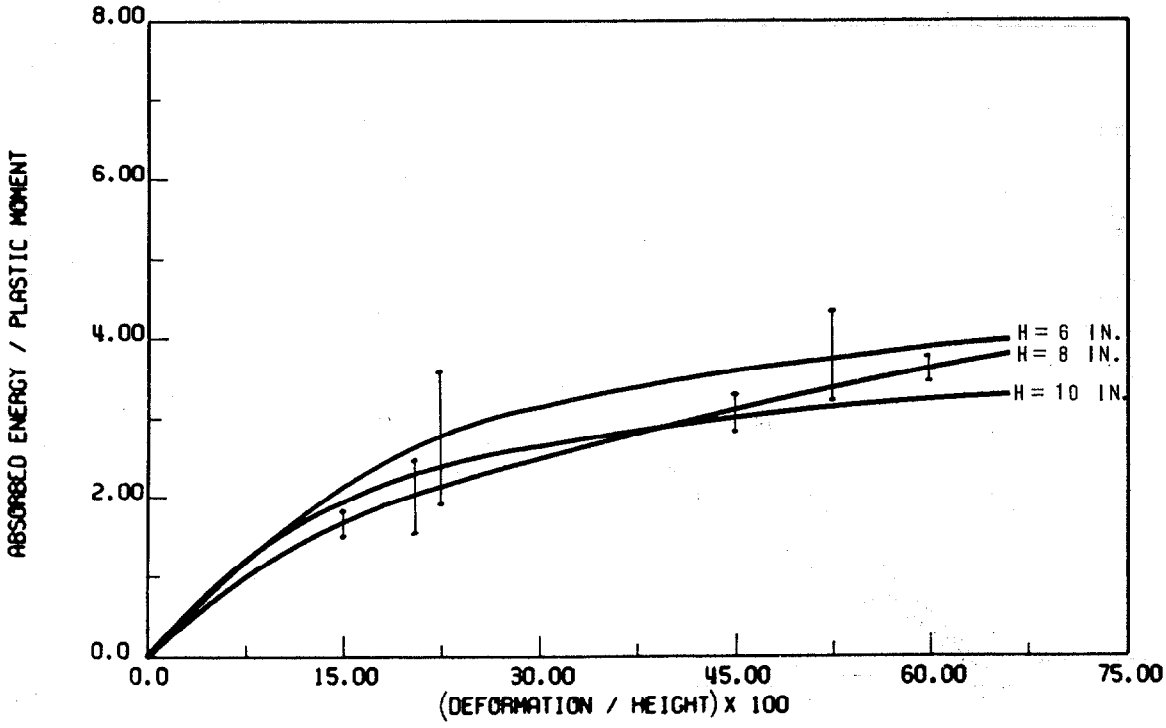

Figure 5.6. The Absorbed Energy Derived From Accelerometer Test Data Divided by the Plastic Moment as a Function of the Percentage of Deformation Experienced by Impacted Specimens With a 20-Degree Angle of Inclination.

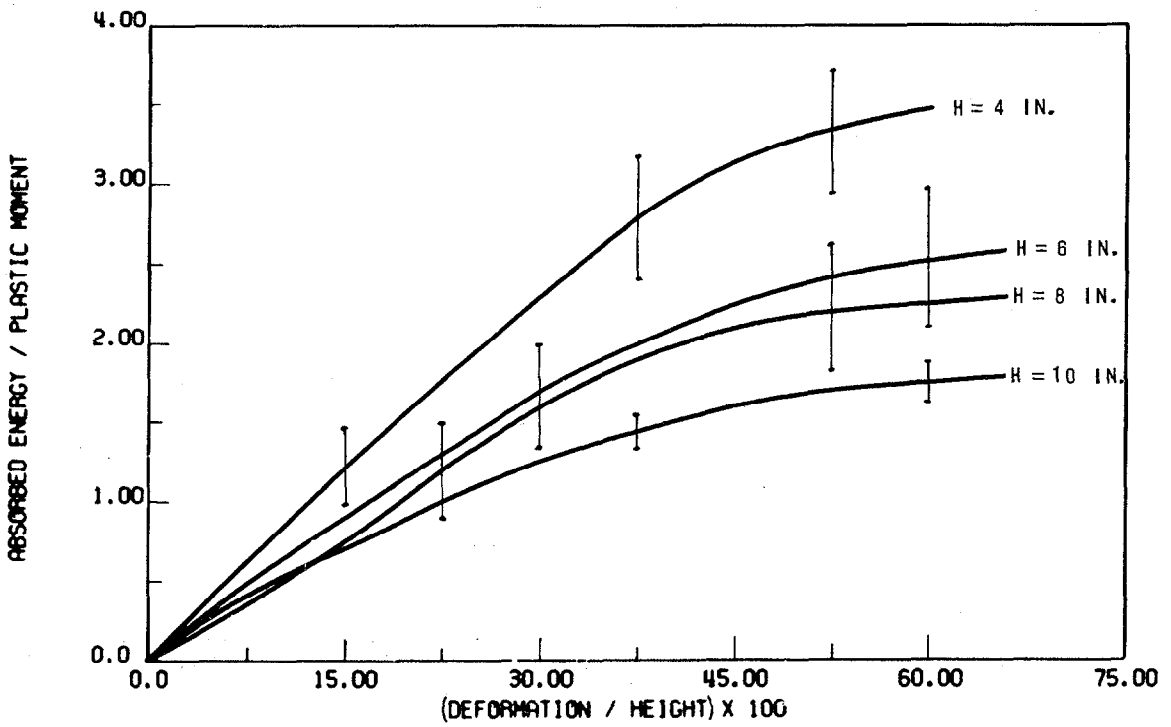

Figure 5.7. The Absorbed Energy Derived From Accelerometer Test Data Divided by the Plastic Moment as a Function of the Percentage of Deformation Experienced by Impacted Specimens With a 30-Degree Angle of Inclination.

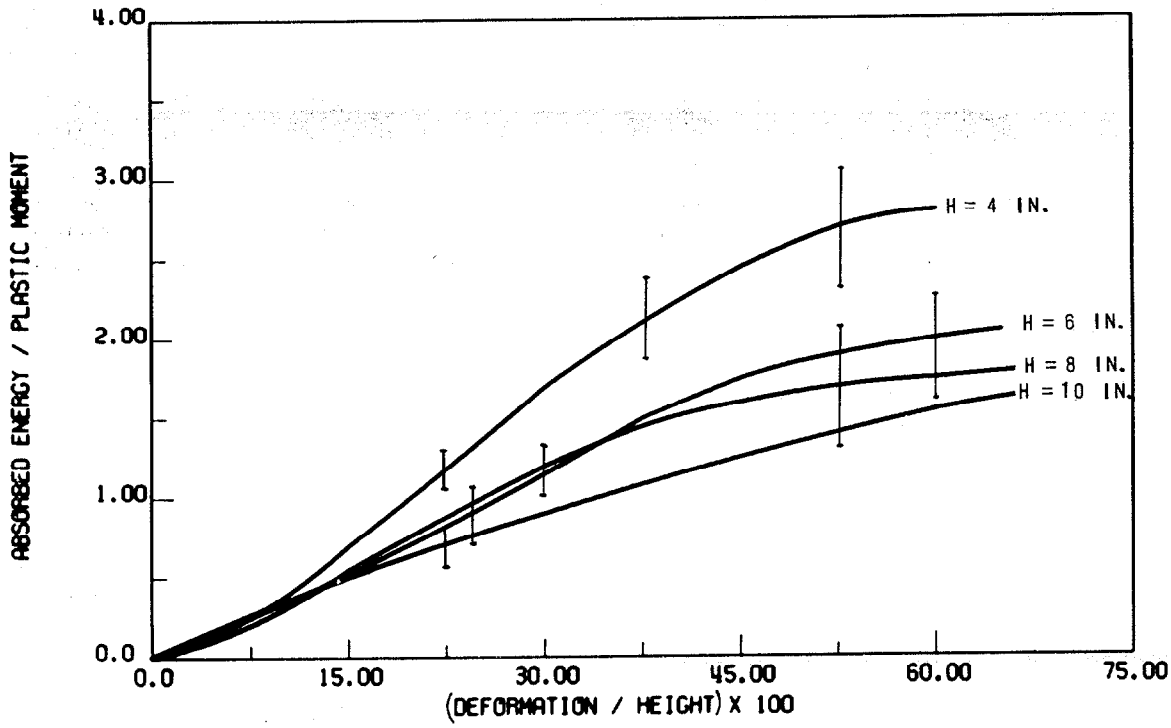

Figure 5.8. The Absorbed Energy Derived From Accelerometer Test Data Divided by the Plastic Moment as a Function of the Percentage of Deformation Experienced by Impacted Specimens With a 40-Degree Angle of Inclination.

double-hinge mode. This indicates that the transition point between single- and double-hinge modes of failure lies between 10 and 20 degrees of inclination.

The typical modes of failure experienced by the test specimens are shown in Figure 5.9. Shown at the top of this photograph are three impact tested specimens that originally had angles of inclination of zero degrees. The left-hand group of three specimens in the second row is comprised of specimens with 10-degree angles of inclination, and the right-hand group is comprised of specimens with 20-degree angles of inclination. Specimens with 30-degree angles of inclination are shown in the left-hand group of three specimens in the bottom row, and specimens with 40-degree angles of inclination are shown in the right-hand group in the bottom row. In each of these groups of three specimens except the first at the top of the photograph, the first specimen shown has not been impact tested and the other two have been tested.

The time durations of the impact events for specimens which failed in a double-hinge mode ran from 2.6 to 22.2 milliseconds, with the majority running from 7 to 15 milliseconds. The durations of impact events for specimens which failed in a single-hinge mode were much longer with some being up to 154 milliseconds. Although the impact durations of single-hinge failures were much longer, they were much less violent than those of the double-hinge failures.

The printed computer output for each specimen tested afforded a means by which the calculated deformation could be compared with the final measured deformation. It also allowed the absorbed energy calculated from the experimental data to be compared with the energy of the

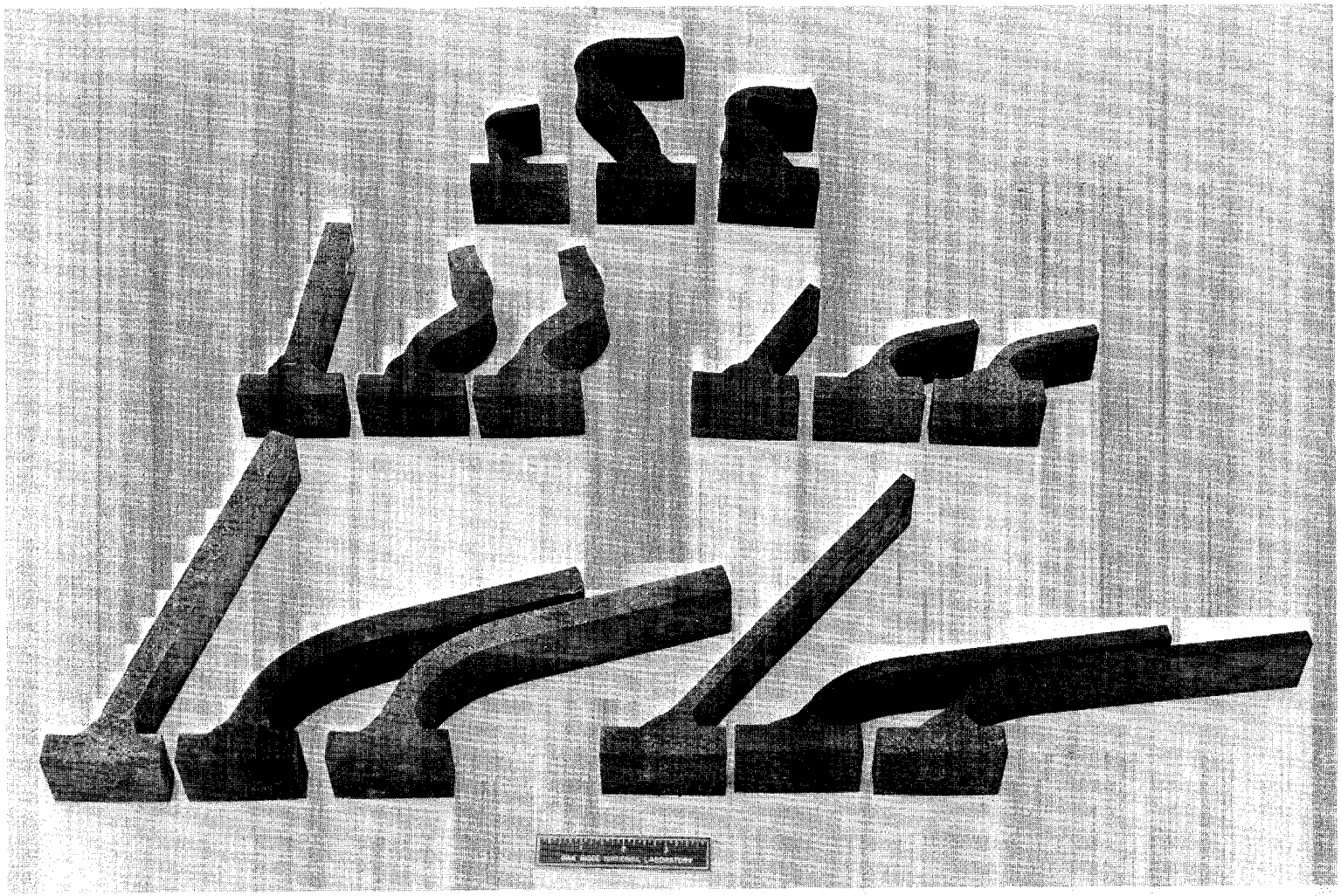

Figure 5.9. Typical Fin Specimens With Angles of Inclination of 0, 10, 20, 30, and 40 Degrees Before and After Impact.

falling hammer at the time of initial impact. The printed computer output for the first ten specimens tested is given in Appendix B. The deviations between the calculated values of deformation and the measured values of final deformation shown in this output are typical for the specimens that failed in a double-hinge mode. These deviations were up to 30 percent from the measured values. Larger deviations were observed for specimens that failed in a single-hinge mode. These deviations are at least partially due to the elastic springback of the specimens when the energy had been dissipated and the load removed, especially for those specimens which failed in a single-hinge mode.

The differences between the energy which was applied to the specimens and the absorbed energy accounted for in the test data were very small, being in the order of 2 to 3 percent. This was true for specimens experiencing either type of failure mode, single or double hinge. A relatively small amount of energy was dissipated by friction in the horizontal motion between the hammer and the top of the specimens as the collapse occurred. The horizontal motions were small for double-hinge failures where the forces between the hammer and the specimens were large, and the horizontal motions were relatively large for single-hinge failures where the forces between the hammer and the specimens were small. Therefore, the energies absorbed by this friction remained relatively small.

The range of data scatter is indicated by the fine vertical lines in the graphical presentation of the computer output. The maximum deviation from the median curves shown in Figures 5.1 through 5.5 (pages 29 through 33) is less than 20 percent with only three exceptions. The

curves shown in these five computer plots were derived from load cell data. The curves derived from the acclerometer data, shown in Figures 5.6 through 5.8 (pages 35 through 37), are well within the data band derived from the load cell data. This correlation between the load cell data and accelerometer data provides a degree of assurance that the results presented are within acceptable engineering accuracy.

Analysis of the curves shown in Figures 5.1 through 5.5 (pages 29 through 33) shows that the energy absorption capabilities of a specimen are dependent upon the square of the thickness of the specimen. This is evidenced by the fact that when the energy absorbed by the specimen was divided by its plastic moment value, which is basically a constant multiplied by the square of the thickness of the specimen, and the value obtained was plotted against the percentage of deformation resulting from the impact; the result for the specimens tested was a set of curves dependent upon specimen height alone. For deformations of 10 percent or less, the results were almost independent of the height of the specimen. This is especially true for the specimens with angles of inclination of 0, 10, and 20 degrees. For larger deformations, it is evident that the specimens with greater heights absorbed less energy for the same percentage of deformation experienced by the specimens with lesser heights.

The computer output for the peak force experienced by the specimens during impact as a function of their height divided by their thickness is represented graphically in Figures 5.10 through 5.14. More data scatter is observable for the specimens with a double-hinge mode of failure than for those with a single-hinge mode. Buckling is the primary mode in double-hinge failures, while bending is the primary mode in

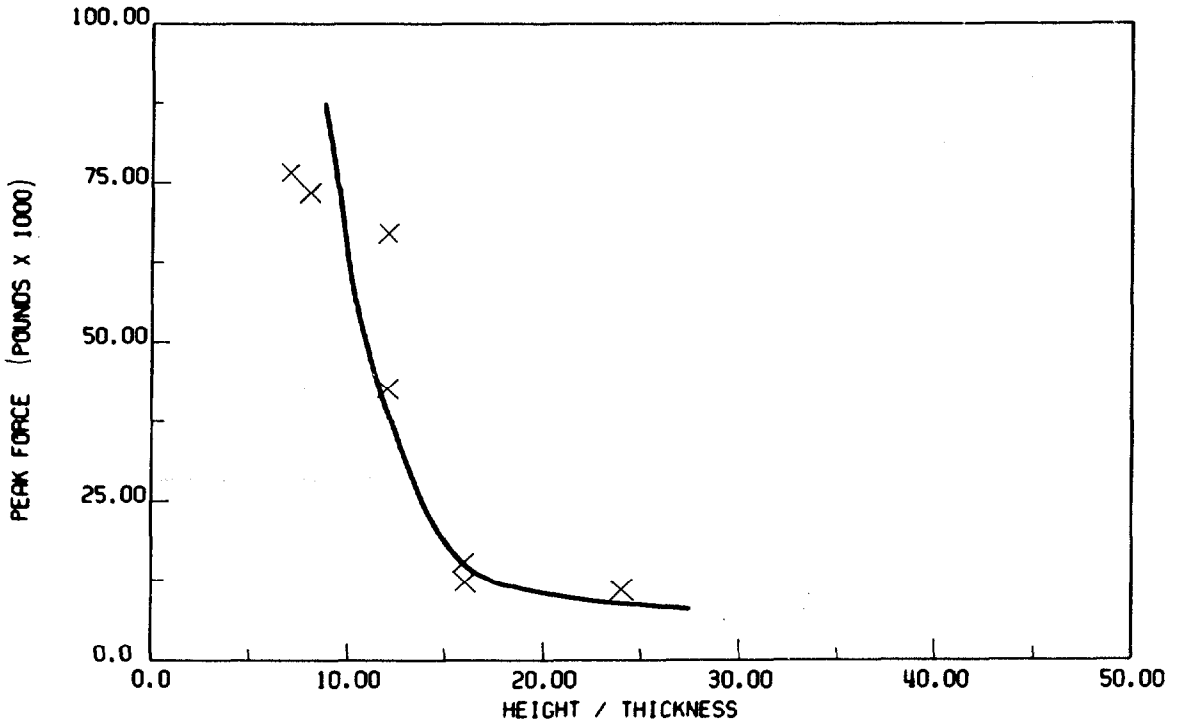

Figure 5.10. The Peak Force Derived From Load Cell Test Data as a Function of Specimen Height Divided by Thickness for Impacted Specimens With a Zero-Degree Angle of Inclination.

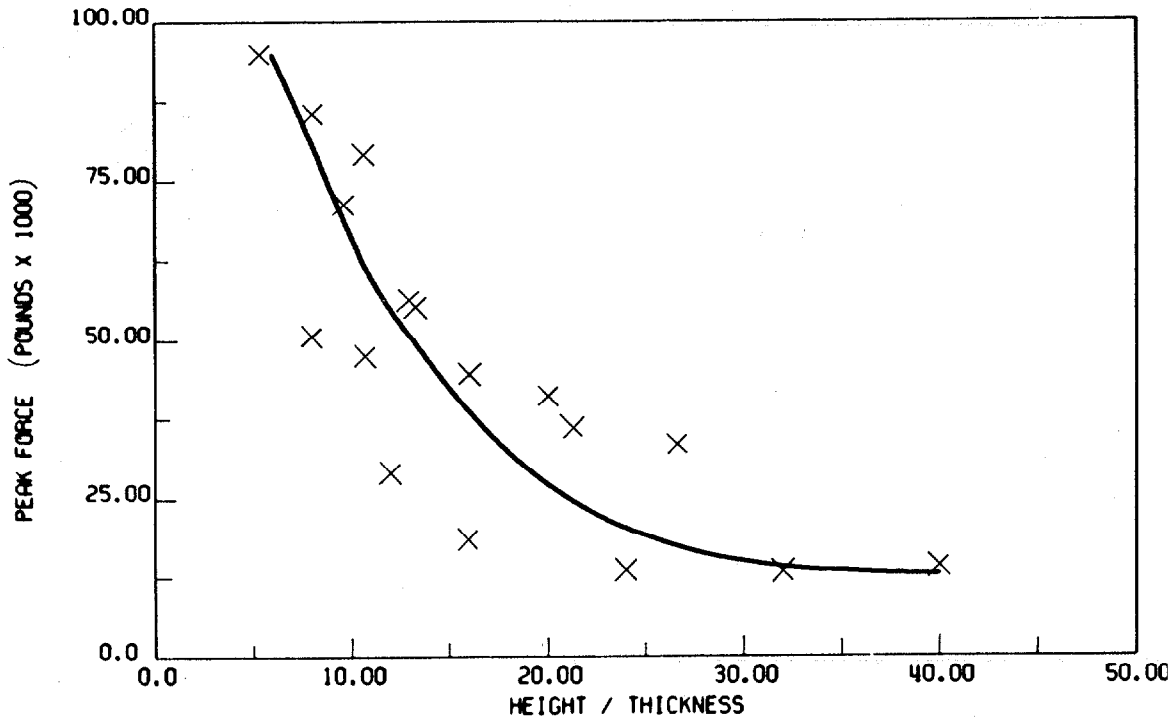

Figure 5.11. The Peak Force Derived From Load Cell Test Data as a Function of Specimen Height Divided by Thickness for Impacted Specimens With a 10-Degree Angle of Inclination.

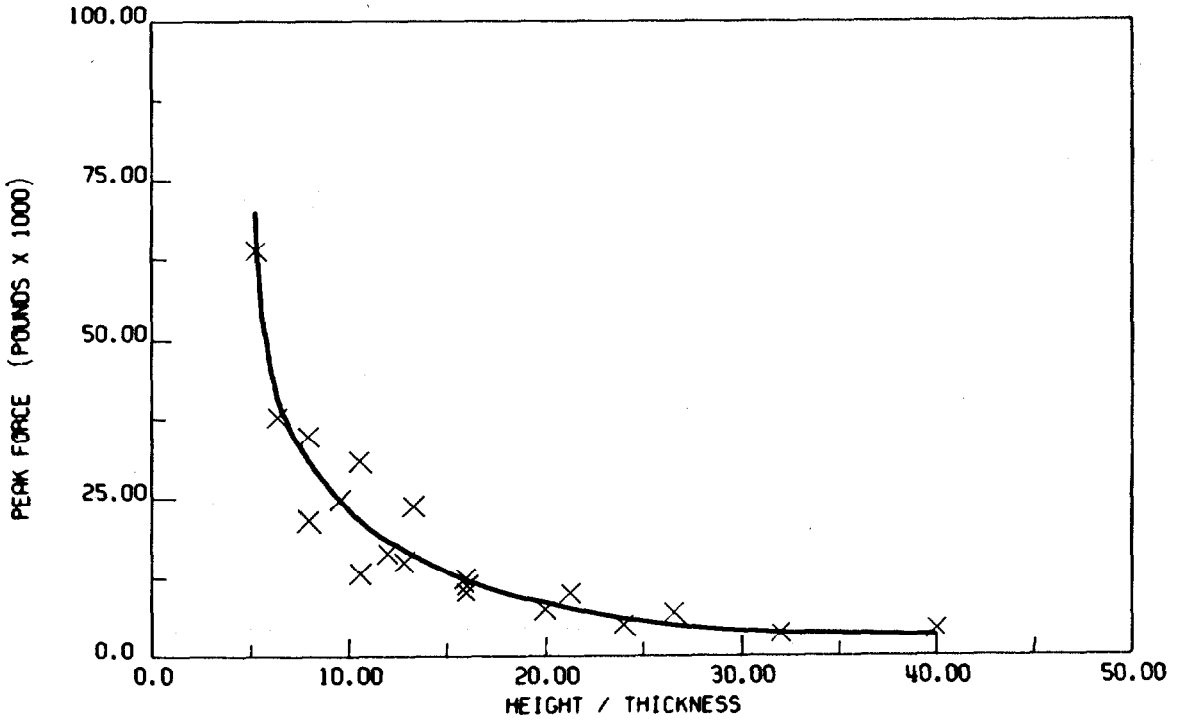

Figure 5.12. The Peak Force Derived From Load Cell Test Data as a Function of Specimen Height Divided by Thickness for Impacted Specimens With a 20-Degree Angle of Inclination.

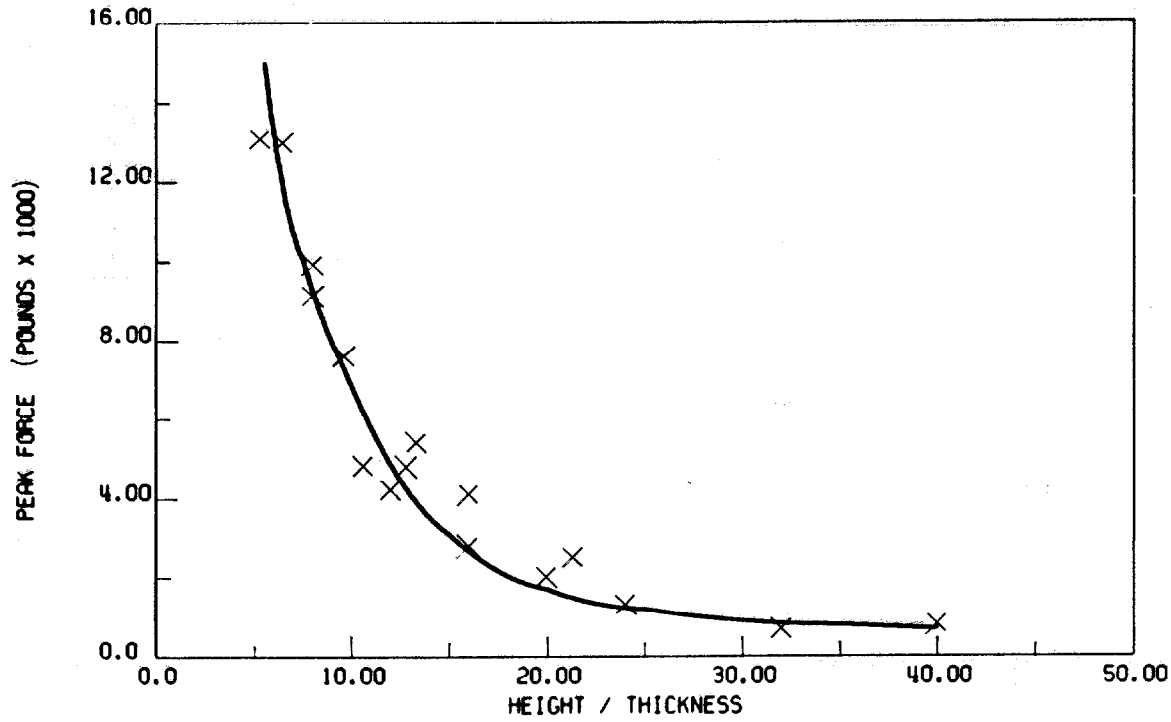

Figure 5.13. The Peak Force Derived From Load Cell Test Data as a Function of Specimen Height Divided by Thickness for Impacted Specimens With a 30-Degree Angle of Inclination.

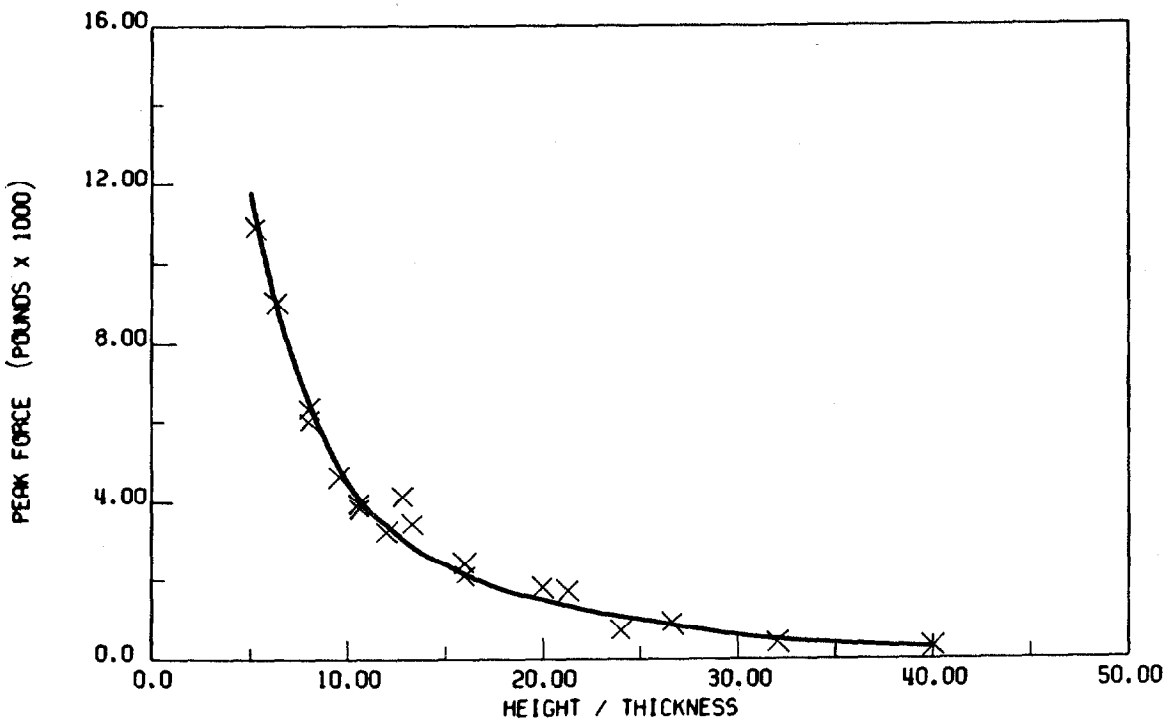

Figure 5.14. The Peak Force Derived From Load Cell Test Data as a Function of Specimen Height Divided by Thickness for Impacted Specimens With a 40-Degree Angle of Inclination.

single-hinge failures. When presented as is done in Figures 5.10 through 5.14, experimental buckling data typically has significant scatter, while experimental bending data is typically more well behaved.

The peak force information was derived solely from the load cell data recorded during the impact tests. A low-pass filter was necessary to remove high-frequency noise from the accelerometer output signal. This filter attenuated the sharp peak acceleration value that actually occurred in the first part of the impact event, and this attenuation may be noted on the typical oscilloscope photographs shown in Figures 4.3 and 4.4 (page 26). Therefore, the peak force values obtained from the accelerometer data were not valid. This attenuation characteristic did not materially affect the energy absorption information derived from the accelerometer data because energy values were obtained by double integration of the acceleration-time data curve.

The peak force values recorded during the impact tests were linearly dependent upon the height and thickness of the specimens tested, as may be observed in Figures 5.10 through 5.14 (pages 42 through 46). These curves are very similar to critical load curves for columns with different length-to-radius-of-gyration ratios. Actually, the height-thickness ratios of the specimens used are essentially height-to-radius-of-gyration ratios since

$$k = \left(\frac{I}{A}\right)^{1/2} = \left(\frac{\frac{bt^3}{12}}{bt}\right)^{1/2} = tC \tag{5.3}$$

where

k = radius of gyration,

I = moment of inertia,

A = area in square inches,

b = length of specimen = 2 inches,

t = thickness of specimen in inches, and

C = a constant.

It was observed many times throughout the impact tests that the peak force value for a given specimen geometry was not dependent on the input energy of the hammer as long as the specimen was plastically deformed. The input energy could be doubled by either doubling the weight of the hammer or the drop height, but the peak force would remain essentially constant. The increased energy was absorbed by more deformation that occurred over a longer duration.

6. CONCLUSIONS AND RECOMMENDATIONS

To summarize before drawing conclusions and making recommendations, 275 specimens of shipping cask fins of different geometries were impact tested to determine the energy absorption capabilities of external longitudinal fins undergoing gross deformation. It was assumed that the energy absorption characteristics of these fins are linear with length, and the length (longitudinal distance of fin along the cask body) of each fin specimen was held constant at 2 inches. The heights (measured from the outside surface of the cask to the fin tip) of the specimens tested varied from 3.5 and 4 to 10 inches in 2-inch increments, and the thicknesses of the specimens varied from 1/4 to 3/4 inch in 1/8-inch increments. The specimens tested had five different angles of inclination: 0, 10, 20, 30, and 40 degrees.

The force experienced by each impacted specimen was measured and recorded as a function of time by using load cells, signal conditioning equipment, an oscilloscope, and photography equipment. Acceleration as a function of time was also measured and recorded during the latter portion of the impact testing by using an accelerometer attached to the hammer in conjunction with appropriate signal conditioning equipment, the oscilloscope, and photography equipment. The force-time and acceleration-time data were transformed into absorbed energy-deformation data by means of a computer program prepared for this purpose, and the results of the impact tests were evaluated.

6.1 Conclusions

The objective of this investigation was to determine the energy absorption characteristics of plastically deformed fin specimens and present the resulting information in a form readily usable by a shipping cask designer or analyst for calculation of the energy absorption characteristics of external fins along the longitudinal axis of a cylindrical cask subjected to the 30-foot free-fall condition of the hypothetical accident specified in the regulations (1,2) governing shipping casks for radioactive and fissile materials. Curves are presented in Figures 5.1 through 5.5 (pages 29 through 33) in Subsection 5.2 that will enable a cask designer or analyst to compute the energy absorption capacity of a longitudinal fin on a shipping cask as a function of its geometry and the percentage of deformation it is expected to experience during an impact.

The energy absorption capacity of a fin specimen was shown to be dependent upon the square of its thickness. The greater the height of the specimen, the less the energy that was absorbed for the same percentage of deformation once that deformation had proceeded into a gross range (10 percent or greater). The fact that the data obtained by two independent methods during the latter portion of the experimental program reduced to similar curves representing the energy absorbed versus the percentage of deformation experienced by the specimens provides a degree of confidence in the results.

The curves shown in Figures 5.10 through 5.14 (pages 42 through 46) in Subsection 5.2 are plots of the peak force experienced by specimens during impact versus their heights divided by their thicknesses. With

the weight of a shipping cask known, the peak acceleration that would be experienced by a cask subjected to the 30-foot free-fall condition of the hypothetical accident can be computed by using the information presented in Figures 5.10 through 5.14 (pages 42 through 46). The peak force values observed during the impact tests were linearly dependent on the height and thickness of the specimens tested, and the plots are similar to critical load curves for columns. The peak force experienced by the specimens did not appear to be a function of the impact energy of the hammer as long as plastic deformation was attained. The intended use of these energy absorption and peak force curves presented in Subsection 5.2 is demonstrated in the example problem given in Appendix C.

The techniques employed during the performance of the impact tests proved to be relatively economical and effective in determining the energy absorption and peak force data for longitudinal fins on shipping casks. These techniques would also be applicable in experimental programs intended to determine the energy absorption capabilities of specimens of other geometries or the dynamic stress-strain relationships of ductile materials.

6.2 Recommendations

It is recommended that the curves shown in Figures 5.1 through 5.5 (pages 29 through 33) be used to determine the energy absorption capabilities of external fins along the longitudinal axis of cylindrical shipping casks being evaluated to determine compliance with the regulations (1,2) governing structural integrity during the 30-foot free-drop hypothetical accident condition. The curves shown in Figures 5.10

through 5.14 (pages 42 through 46) may be used to determine the peak forces to which the cask fins would be subjected under the same accident condition.

Considerably more impact testing should be done with regard to the energy absorption characteristics of cask fins to adequately provide all of the information on this subject presently needed by designers and analysts of shipping casks for radioactive and fissile materials. Inquiries have already been received relative to data for fin geometries much larger than those tested. These large geometries include fin thicknesses up to 1 1/4 inches and heights up to 18 inches. Extrapolation of the results presented here to fin geometries grossly different from those evaluated could give erroneous information. A test program should be conducted to substantiate the assumption that the energy absorption characteristics of longitudinal fins vary linearly with their length.

It is recommended that fin specimens of materials other than that tested in this investigation be evaluated, with special interest being directed to specimens fabricated of a 300-series stainless steel. Tests should also be conducted to evaluate the energy absorption characteristics of circumferential fins. The need for these two types of investigations is very real inasmuch as inquiries have been received as to whether the results of this investigation will be applicable to these particular situations. The results of this investigation should not be applied to circumferential fins or fins of other materials without further investigation. A study should be undertaken to develop an analytical approach for direct computation of the energy absorbed by a cask fin during impact as a function of its deformation, and the results

obtained by using this analytical method could then be correlated with the experimental results presented here.

Finally, it is recommended that the energy absorption characteristics of pre-bent fins be evaluated. This type of fin geometry would tend to reduce the extremely high peak forces that are experienced when a straight fin is dynamically deformed at no angle or a shallow angle of impact inclination. The pre-bent type of fin should absorb nearly as much energy as the straight fin under these circumstances since the double-hinge mode would still be the effective mode of failure.

LIST OF REFERENCES

1. United States Atomic Energy Commission Manual, Volume 0000, General Administration, Part 0500, Health and Safety, Chapter 0529, Safety Standards for the Packaging of Radioactive or Fissile Materials, August 22, 1966.

2. Code of Federal Regulations, Title 10, Part 71, Transport of Licensed Materials; also see Federal Register, Vol. 31, pp. 9941-9949, July 1966.

3. G. R. Abrahamson and J. N. Goodier, "Dynamic Flexural Buckling of Rods Within an Axial Plastic Compression Wave," Transactions of the ASME, Series E: Journal Of Applied Mechanics, pp. 241-247, June 1966.

4. B. Rawlings, "Energy Absorption of Dynamically and Statically Tested Mild Steel Beams Under Conditions of Gross Deformation," International Journal of Mechanical Sciences, Vol. 9, pp. 633-649, 1967.

5. E. W. Parkes, "The Permanent Deformation of a Cantilever Struck Transversely At Its Tip," Proceedings of the Royal Society (London), Series A, Vol. 228, pp. 462-476, 1955.

6. S. R. Bodner and P. S. Symonds, "Plastic Deformations in Impact and Implusive Loading of Beams," Plasticity, Proceedings of the Second Symposium on Naval Structural Mechanics, pp. 488-500, Pergamon Press, 1960.

7. T. C. T. Ting, "Large Deformation of a Rigid, Ideally Plastic Cantilever Beam," Transactions of the ASME, Series E: Journal of Applied Mechanics, pp. 295-302, June 1965.

APPENDIX A

LOAD CELL CALIBRATION CURVES

The load cells used in the experimental program had maximum capacities of 16,000, 32,000, 120,000, and 300,000 pounds. These cells were calibrated by using a Baldwin 120,000-pound hydraulic compression testing machine, as discussed in Subsection 3.3, and the calibration curves for the load cells are illustrated in Figures A.1 through A.4.

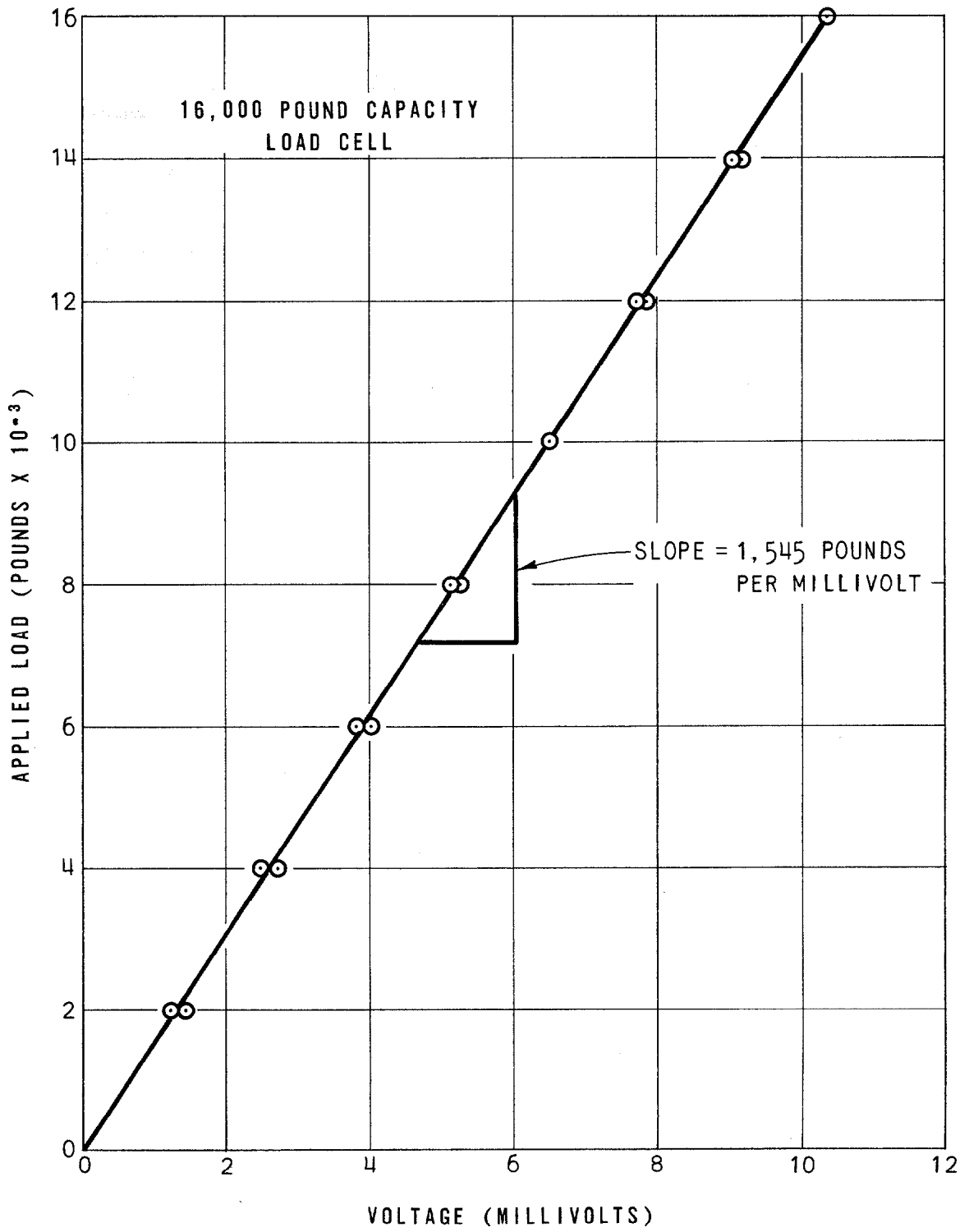

Figure A.1. Calibration Curve for the Load Cell With a Maximum Capacity of 16,000 Pounds.

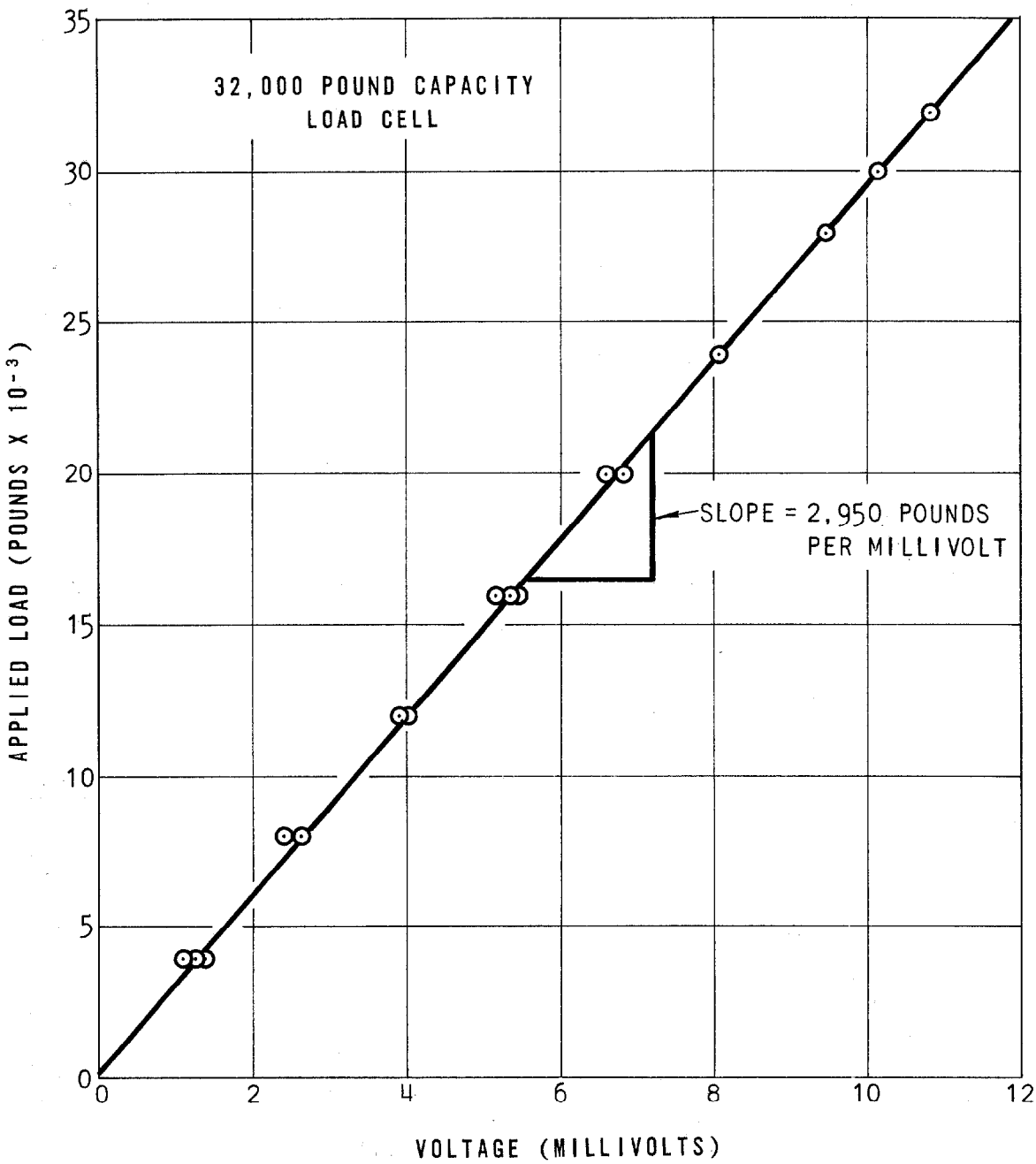

Figure A.2. Calibration Curve for the Load Cell With a Maximum Capacity of 32,000 Pounds.

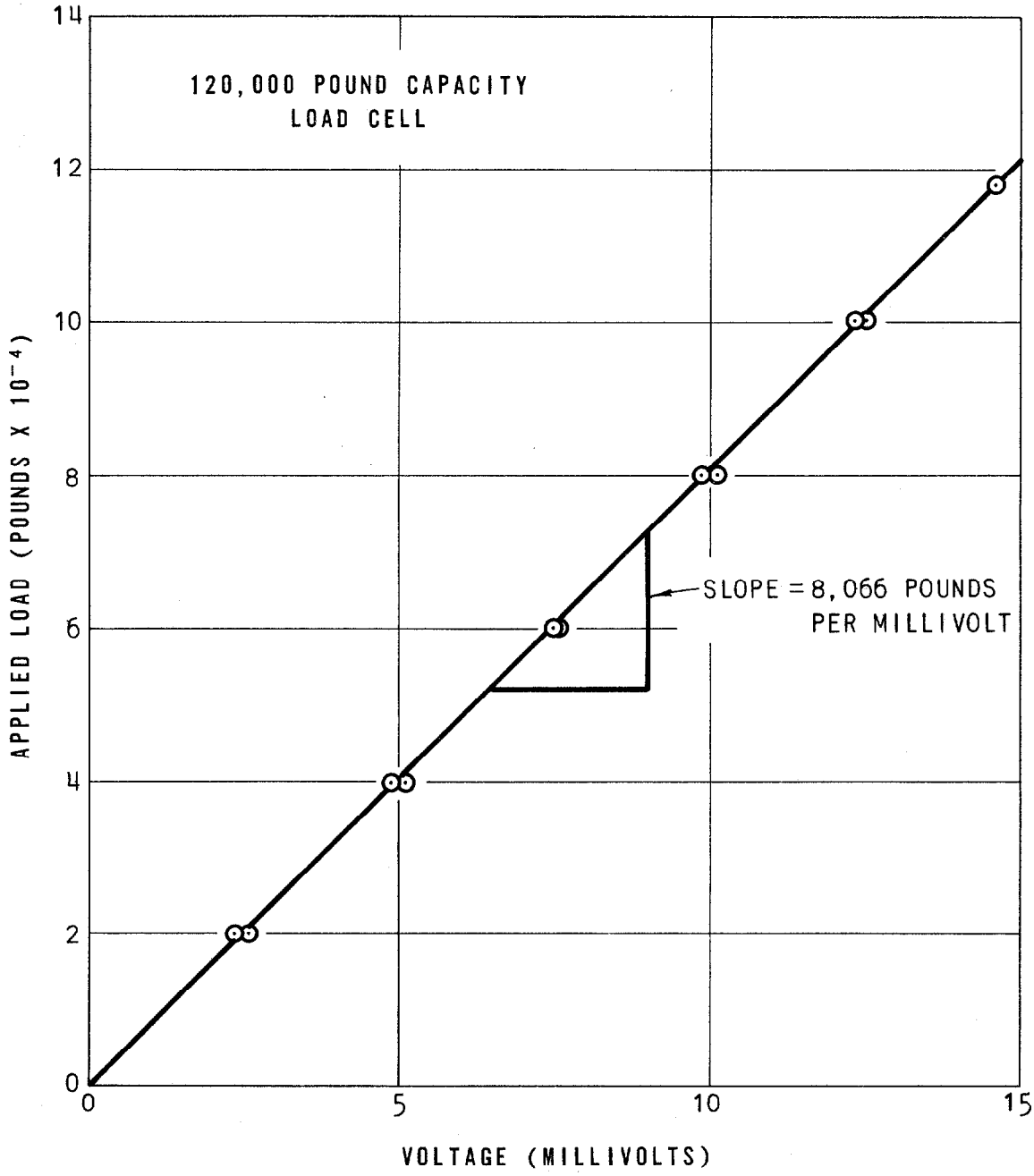

Figure A.3. Calibration Curve for the Load Cell With a Maximum Capacity of 120,000 Pounds.

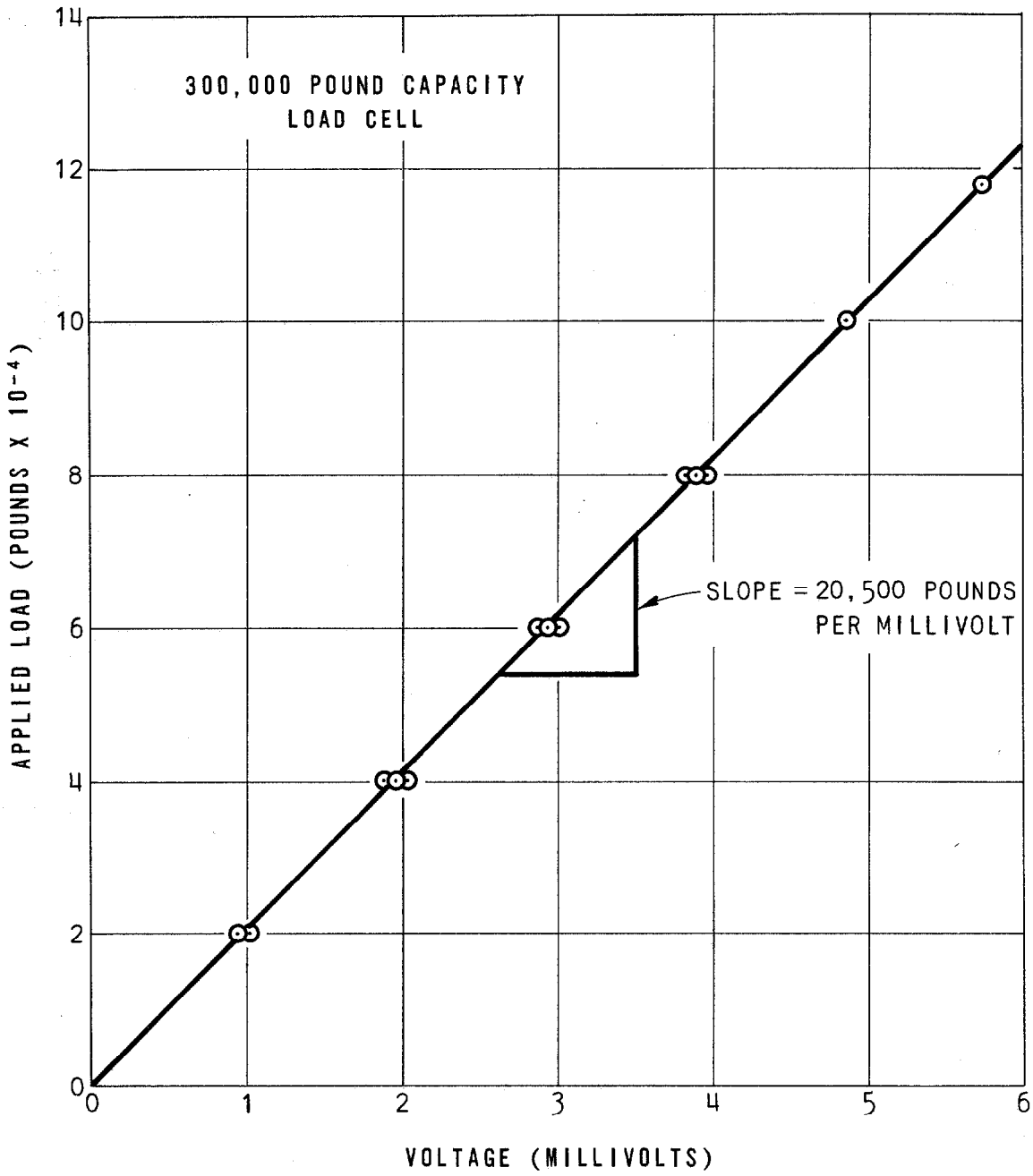

Figure A.4. Calibration Curve for the Load Cell With a Maximum Capacity of 300,000 Pounds.

APPENDIX B

DATA TRANSFORMATION COMPUTER PROGRAM

A Fortran program applicable to the IBM 360 computer at Oak Ridge National Laboratory was prepared to transform the force-time and acceleration-time data recorded during the impact tests into absorbed energy-deformation data. This program, which is discussed in Subsection 5.1, is presented on the following pages.

```
C THIS PROGRAM TRANSFORMS FORCE-TIME DATA INTO ABSORBED ENERGY-TIME
C RELATIONSHIPS FOR FIN SPECIMENS IMPACTED BY A FREE FALLING WEIGHT.
C CODED BY F C DAVIS OAK RIDGE NATL LAB DECEMBER 1969
C              GLOSSARY OF NOTATION
C              I=SPECIMEN IDENTIFICATION NUMBER
C              J=DATA POINT IDENTIFICATION NUMBER
C              NN=NUMBER OF DATA POINTS PER SPECIMEN
C              F=FORCE IN POUNDS
C              A=ACCELERATION IN FT/SEC/SEC
C              EL=ELEVATION IN INCHES
C              W=WEIGHT OF IMPACT HAMMER IN POUNDS
C              VO=VELOCITY OF HAMMER AT T=0 SEC IN FEET/SEC
C              V=VELOCITY AT ANY POINT IN TIME IN FEET/SEC
C              T=TIME AFTER IMPACT IN SEC
C              TK=SPECIMEN THICKNESS IN INCHES
C              H=SPECIMEN HEIGHT IN INCHES
C              ANG=SPECIMEN ANGLE IN DEGREES
C              D=VERTICAL DIMENSION AFTER IMPACT IN INCHES (MEASURED)
C              X=ACTUAL VERTICAL DEFORMATION IN INCHES
C              UI=ENERGY OF HAMMER AT IMPACT IN IN-LBS
C              U=ENERGY ABSORBED AT ANY POINT IN TIME IN IN-LBS
C              MP=PLASTIC MOMENT OF SPECIMEN CROSS SECTION IN IN-LBS
C              UMP=ABSORBED ENERGY / PLASTIC MOMENT
C              DEF=CALCULATED DEFORMATION AT ANY POINT IN TIME IN INCHES
C              PDEF=CALCULATED DEFORMATION / ORIGINAL HEIGHT X 100
C              NS=NUMBER OF SPECIMENS
C              INO=INITIAL SPECIMEN NUMBER FOR GROUP BEING COMPUTED
      DIMENSION F(25,50),A(25,50),EL(25),W(25),VO(25),V(25,50),NN(25),
     1T(25,50),TK(25),H(25),ANG(25),D(25),X(25),UI(25),U(25,50),MP(25),
     2UMP(25,50),DEF(25,50),PDEF(25,50)
 1001 FORMAT (I2,F18.1,5F10.1/(F20.1,5F10.1))
 1002 FORMAT (I2,F18.5,5F10.5/(F20.5,5F10.5))
 1003 FORMAT (7F10.1/(7F10.1))
 1004 FORMAT (7F10.2/(7F10.2))
 1005 FORMAT (7F10.3/(7F10.3))
 1006 FORMAT (I5)
```

```
C ZERO STORAGE REGISTERS FOR ALL SUBSCRIPTED VARIABLES
      DO 1 I=1,25
      EL(I)=0.0
      W(I)=0.0
      VO(I)=0.0
      NN(I)=0.0
      TK(I)=0.0
      H(I)=0.0
      ANG(I)=0.0
      D(I)=0.0
      X(I)=0.0
      UI(I)=0.0
 1    MP(I)=0.0
      DO 2 I=1,25
      DO 2 J=1,50
      F(I,J)=0.0
      A(I,J)=0.0
      V(I,J)=0.0
      T(I,J)=0.0
      U(I,J)=0.0
      UMP(I,J)=0.0
      DEF(I,J)=0.0
 2    PDEF(I,J)=0.0
C READ IN TEST DATA
      READ 1006,NS
      READ 1006,INO
      DO 3 I=1,NS
      READ 1001,N,(F(I,J),J=1,N)
      READ 1002,N,(T(I,J),J=1,N)
 3    NN(I)=N
      READ 1003,(EL(I),I=1,NS)
      READ 1003,(W(I),I=1,NS)
      READ 1004,(H(I),I=1,NS)
      READ 1005,(D(I),I=1,NS)
      READ 1005,(TK(I),I=1,NS)
      READ 1004,(ANG(I),I=1,NS)
```

```
C CONVERT FORCE-TIME DATA TO ACCELERATION-TIME DATA
      DO 5 I=1,NS
      DO 4 J=1,NN(I)
 4    A(I,J)=(F(I,J)*32.0)/W(I)
 5    CONTINUE
C COMPUTE VELOCITY OF HAMMER AT IMPACT WHERE T=0
      DO 6 I=1,NS
 6    VO(I)=SQRT(64.0*EL(I)/12.0)
C COMPUTE VELOCITY-TIME DATA BY INTERGATING THE ACCEL-TIME CURVE
      DO 9 I=1,NS
      SUMA=0.0
      DO 8 J=1,NN(I)
      IF (J.EQ.1) GO TO 7
      SUMA = SUMA+((T(I,J)-T(I,J-1))*(A(I,J-1)+A(I,J)))/2.0
 7    V(I,J)=VO(I)-SUMA
 8    IF (V(I,J).LE.0.0) NN(I)=J-1
 9    CONTINUE
C COMPUTE DEFORMATION-TIME DATA BY INTEGRATING THE VELOCITY-TIME CURVE
      DO 12 I=1,NS
      SUMV=0.0
      DO 11 J=1,NN(I)
      IF (J.EQ.1) GO TO 10
      SUMV = SUMV+((T(I,J)-T(I,J-1))*(V(I,J-1)+V(I,J)))/2.0
 10   DEF(I,J)=SUMV*12.0
      B=(H(I)*COS(ANG(I)/57.3))-DEF(I,J)
      IF (B.LE.0.0) NN(I)=J-1
      IF (NN(I).EQ.(J-1)) GO TO 11
C CALCULATE PERCENTAGE DEFORMATION
 11   PDEF(I,J)=DEF(I,J)*100.0/H(I)
 12   CONTINUE
C CALCULATE ACTUAL FINAL DEFORMATION FROM MEASUREMENTS
      DO 13 I=1,NS
 13   X(I)=(H(I)*COS(ANG(I)/57.3))-D(I)
C CALCULATE ENERGY OF HAMMER AT IMPACT
      DO 14 I=1,NS
 14   UI(I)=EL(I)*W(I)
```

```
C COMPUTE ABSORBED ENERGY FROM FORCE-DEFORMATION DATA
      DO 16 I=1,NS
      SUME=0.0
      DO 15 J=1,NN(I)
      IF (J.EQ.1) GO TO 15
      SUME = SUME+((DEF(I,J)-DEF(I,J-1))*(F(I,J)+F(I,J-1)))/2.0
 15   U(I,J)=SUME
 16   CONTINUE
C CALCULATE PLASTIC MOMENT FOR FIN SPECIMENS, WIDTH OF SECTION = 2IN
C AND YEILD STRESS = 30,000 PSI
      DO 17 I=1,NS
 17   MP(I)=15000.*TK(I)*TK(I)
C COMPUTE RATIO ABSORBED ENERGY / PLASTIC MOMENT
      DO 19 I=1,NS
      DO 18 J=1,NN(I)
 18   UMP(I,J)=U(I,J)/MP(I)
 19   CONTINUE
C COMPUTE SPECIMEN IDENTIFICATION NUMBER
      DO 22 I=1,10
 20   ISPEC=INO+I
      WRITE (51,1007)
 1007 FORMAT ( 1H1,10X,1HI,4X,2HHT,4X,3HTHK,3X,3HANG,4X,2HWT,4X,3HELE,
     15X,4HTIME,4X,5HFORCE,5X,3HDEF,5X,4HMEAS,4X,5HCAL U,5X,4HU IN)
      WRITE (51,1008)
 1008 FORMAT ( 1H ,14X,4H(IN),2X,4H(IN),2X,5H(DEG),2X,4H(LB),3X,4H(IN),
     13X,5H(SEC),5X,4H(LB),5X,4H(IN),4X,4H(IN),3X,7H(IN-LB),3X,7H(IN-LB)
     2)
      WRITE (51,1009)
 1009 FORMAT (1H )
      DO 21 J=1,NN(I)
 21   WRITE (51,1010) ISPEC,H(I),TK(I),ANG(I),W(I),EL(I),T(I,J),F(I,J),
     1DEF(I,J),X(I),U(I,J),UI(I)
 1010 FORMAT (10X,I2,3X,F3.1,3X,F4.3,3X,F3.0,3X,F4.0,3X,F4.0,3X,F5.4,3X,
     1F7.0,3X,F5.3,3X,F5.3,3X,F7.0,3X,F7.0)
 22   CONTINUE
      STOP
```

I	HT (IN)	THK (IN)	ANG (DEG)	WT (LB)	ELE (IN)	TIME (SEC)	FORCE (LB)	DEF (IN)	MEAS (IN)	CAL U (IN-LB)	U IN (IN-LB)
1	6.0	.750	0.	474.	354.	.0	153750.	0.0	2.625	0.	167915.
1	6.0	.750	0.	474.	354.	.0002	143500.	0.102	2.625	15147.	167915.
1	6.0	.750	0.	474.	354.	.0004	133250.	0.199	2.625	28605.	167915.
1	6.0	.750	0.	474.	354.	.0006	92250.	0.292	2.625	39113.	167915.
1	6.0	.750	0.	474.	354.	.0008	82000.	0.382	2.625	46950.	167915.
1	6.0	.750	0.	474.	354.	.0012	82000.	0.554	2.625	61035.	167915.
1	6.0	.750	0.	474.	354.	.0014	71750.	0.636	2.625	67337.	167915.
1	6.0	.750	0.	474.	354.	.0016	71750.	0.716	2.625	73047.	167915.
1	6.0	.750	0.	474.	354.	.0018	66625.	0.793	2.625	78394.	167915.
1	6.0	.750	0.	474.	354.	.0020	61500.	0.868	2.625	83207.	167915.
1	6.0	.750	0.	474.	354.	.0022	66625.	0.941	2.625	87887.	167915.
1	6.0	.750	0.	474.	354.	.0024	61500.	1.012	2.625	92434.	167915.
1	6.0	.750	0.	474.	354.	.0026	56375.	1.081	2.625	96500.	167915.
1	6.0	.750	0.	474.	354.	.0028	51250.	1.148	2.625	100114.	167915.
1	6.0	.750	0.	474.	354.	.0030	56375.	1.214	2.625	103634.	167915.
1	6.0	.750	0.	474.	354.	.0032	51250.	1.277	2.625	107061.	167915.
1	6.0	.750	0.	474.	354.	.0034	46125.	1.339	2.625	110080.	167915.
1	6.0	.750	0.	474.	354.	.0036	41000.	1.400	2.625	112716.	167915.
1	6.0	.750	0.	474.	354.	.0046	41000.	1.682	2.625	124296.	167915.
1	6.0	.750	0.	474.	354.	.0048	35875.	1.735	2.625	126316.	167915.
1	6.0	.750	0.	474.	354.	.0050	35875.	1.786	2.625	128158.	167915.
1	6.0	.750	0.	474.	354.	.0052	30750.	1.836	2.625	129831.	167915.
1	6.0	.750	0.	474.	354.	.0054	25625.	1.886	2.625	131218.	167915.
1	6.0	.750	0.	474.	354.	.0056	25625.	1.934	2.625	132457.	167915.
1	6.0	.750	0.	474.	354.	.0058	20500.	1.982	2.625	133554.	167915.
1	6.0	.750	0.	474.	354.	.0074	20500.	2.338	2.625	140857.	167915.
1	6.0	.750	0.	474.	354.	.0076	15375.	2.379	2.625	141603.	167915.
1	6.0	.750	0.	474.	354.	.0078	15375.	2.420	2.625	142234.	167915.
1	6.0	.750	0.	474.	354.	.0080	10250.	2.461	2.625	142754.	167915.
1	6.0	.750	0.	474.	354.	.0082	0.	2.501	2.625	142961.	167915.

I	HT (IN)	THK (IN)	ANG (DEG)	WT (LB)	ELE (IN)	TIME (SEC)	FORCE (LB)	DEF (IN)	MEAS (IN)	CAL U (IN-LB)	U IN (IN-LB)
2	6.0	.750	0.	474.	354.	.0	155000.	0.0	2.000	0.	167915.
2	6.0	.750	0.	474.	354.	.0004	125050.	0.200	2.000	27944.	167915.
2	6.0	.750	0.	474.	354.	.0008	94300.	0.383	2.000	48056.	167915.
2	6.0	.750	0.	474.	354.	.0012	92250.	0.553	2.000	63934.	167915.
2	6.0	.750	0.	474.	354.	.0016	77900.	0.712	2.000	77433.	167915.
2	6.0	.750	0.	474.	354.	.0020	71750.	0.860	2.000	88530.	167915.
2	6.0	.750	0.	474.	354.	.0024	63550.	0.999	2.000	97938.	167915.
2	6.0	.750	0.	474.	354.	.0028	57400.	1.130	2.000	105846.	167915.
2	6.0	.750	0.	474.	354.	.0032	51250.	1.253	2.000	112546.	167915.
2	6.0	.750	0.	474.	354.	.0036	47150.	1.370	2.000	118283.	167915.
2	6.0	.750	0.	474.	354.	.0040	47150.	1.480	2.000	123488.	167915.
2	6.0	.750	0.	474.	354.	.0044	45100.	1.585	2.000	128300.	167915.
2	6.0	.750	0.	474.	354.	.0048	45100.	1.683	2.000	132738.	167915.
2	6.0	.750	0.	474.	354.	.0052	43050.	1.776	2.000	136821.	167915.
2	6.0	.750	0.	474.	354.	.0056	45100.	1.863	2.000	140652.	167915.
2	6.0	.750	0.	474.	354.	.0060	43050.	1.944	2.000	144232.	167915.
2	6.0	.750	0.	474.	354.	.0064	38950.	2.020	2.000	147335.	167915.
2	6.0	.750	0.	474.	354.	.0072	38950.	2.156	2.000	152632.	167915.
2	6.0	.750	0.	474.	354.	.0076	36900.	2.216	2.000	154926.	167915.
2	6.0	.750	0.	474.	354.	.0092	36900.	2.410	2.000	162078.	167915.
2	6.0	.750	0.	474.	354.	.0096	32800.	2.446	2.000	163355.	167915.
2	6.0	.750	0.	474.	354.	.0100	30750.	2.479	2.000	164382.	167915.
2	6.0	.750	0.	474.	354.	.0104	28700.	2.507	2.000	165224.	167915.
2	6.0	.750	0.	474.	354.	.0108	22550.	2.532	2.000	165858.	167915.
2	6.0	.750	0.	474.	354.	.0112	16400.	2.554	2.000	166283.	167915.
2	6.0	.750	0.	474.	354.	.0116	8200.	2.573	2.000	166526.	167915.
2	6.0	.750	0.	474.	354.	.0120	6150.	2.592	2.000	166659.	167915.
2	6.0	.750	0.	474.	354.	.0124	0.	2.610	2.000	166714.	167915.

I	HT (IN)	THK (IN)	ANG (DEG)	WT (LB)	ELE (IN)	TIME (SEC)	FORCE (LB)	DEF (IN)	MEAS (IN)	CAL U (IN-LB)	U IN (IN-LB)
3	6.0	.750	0.	474.	354.	.0	153750.	0.0	2.563	0.	167915.
3	6.0	.750	0.	474.	354.	.0004	106600.	0.200	2.563	26061.	167915.
3	6.0	.750	0.	474.	354.	.0008	92250.	0.386	2.563	44487.	167915.
3	6.0	.750	0.	474.	354.	.0012	75850.	0.559	2.563	59064.	167915.
3	6.0	.750	0.	474.	354.	.0016	67650.	0.722	2.563	70783.	167915.
3	6.0	.750	0.	474.	354.	.0020	61500.	0.877	2.563	80760.	167915.
3	6.0	.750	0.	474.	354.	.0024	55350.	1.023	2.563	89320.	167915.
3	6.0	.750	0.	474.	354.	.0028	51250.	1.163	2.563	96744.	167915.
3	6.0	.750	0.	474.	354.	.0032	47150.	1.295	2.563	103270.	167915.
3	6.0	.750	0.	474.	354.	.0036	41000.	1.422	2.563	108850.	167915.
3	6.0	.750	0.	474.	354.	.0044	41000.	1.659	2.563	118561.	167915.
3	6.0	.750	0.	474.	354.	.0048	36900.	1.769	2.563	122868.	167915.
3	6.0	.750	0.	474.	354.	.0052	34850.	1.875	2.563	126662.	167915.
3	6.0	.750	0.	474.	354.	.0056	38950.	1.976	2.563	130389.	167915.
3	6.0	.750	0.	474.	354.	.0060	20500.	2.073	2.563	133264.	167915.
3	6.0	.750	0.	474.	354.	.0064	14350.	2.166	2.563	134895.	167915.
3	6.0	.750	0.	474.	354.	.0068	16400.	2.258	2.563	136303.	167915.
3	6.0	.750	0.	474.	354.	.0072	22550.	2.347	2.563	138041.	167915.
3	6.0	.750	0.	474.	354.	.0076	20500.	2.434	2.563	139905.	167915.
3	6.0	.750	0.	474.	354.	.0080	20500.	2.518	2.563	141625.	167915.
3	6.0	.750	0.	474.	354.	.0084	16400.	2.599	2.563	143126.	167915.
3	6.0	.750	0.	474.	354.	.0088	16400.	2.678	2.563	144423.	167915.
3	6.0	.750	0.	474.	354.	.0092	14350.	2.755	2.563	145607.	167915.
3	6.0	.750	0.	474.	354.	.0096	16400.	2.830	2.563	146761.	167915.
3	6.0	.750	0.	474.	354.	.0100	20500.	2.903	2.563	148105.	167915.
3	6.0	.750	0.	474.	354.	.0104	16400.	2.974	2.563	149406.	167915.
3	6.0	.750	0.	474.	354.	.0108	16400.	3.042	2.563	150524.	167915.
3	6.0	.750	0.	474.	354.	.0112	14350.	3.108	2.563	151541.	167915.
3	6.0	.750	0.	474.	354.	.0120	14350.	3.234	2.563	153357.	167915.
3	6.0	.750	0.	474.	354.	.0124	12300.	3.295	2.563	154164.	167915.
3	6.0	.750	0.	474.	354.	.0136	12300.	3.467	2.563	156279.	167915.
3	6.0	.750	0.	474.	354.	.0140	14350.	3.521	2.563	156999.	167915.

3	6.0	.750	0.	474.	354.	.0144	16400.	3.573	2.563	157802.	167915.
3	6.0	.750	0.	474.	354.	.0148	16400.	3.623	2.563	158624.	167915.
3	6.0	.750	0.	474.	354.	.0152	18450.	3.671	2.563	159460.	167915.
3	6.0	.750	0.	474.	354.	.0156	16400.	3.717	2.563	160256.	167915.
3	6.0	.750	0.	474.	354.	.0160	12300.	3.761	2.563	160882.	167915.
3	6.0	.750	0.	474.	354.	.0164	8200.	3.803	2.563	161313.	167915.
3	6.0	.750	0.	474.	354.	.0168	6150.	3.844	2.563	161606.	167915.
3	6.0	.750	0.	474.	354.	.0172	4100.	3.884	2.563	161811.	167915.
3	6.0	.750	0.	474.	354.	.0176	4100.	3.923	2.563	161973.	167915.
3	6.0	.750	0.	474.	354.	.0180	0.	3.962	2.563	162054.	167915.

I	HT (IN)	THK (IN)	ANG (DEG)	WT (LB)	ELE (IN)	TIME (SEC)	FORCE (LB)	DEF (IN)	MEAS (IN)	CAL U (IN-LB)	U IN (IN-LB)
4	6.0	.750	0.	474.	354.	.0	135300.	0.0	1.750	0.	167915.
4	6.0	.750	0.	474.	354.	.0004	123000.	0.200	1.750	25865.	167915.
4	6.0	.750	0.	474.	354.	.0008	106600.	0.385	1.750	47041.	167915.
4	6.0	.750	0.	474.	354.	.0012	102500.	0.555	1.750	64839.	167915.
4	6.0	.750	0.	474.	354.	.0016	92250.	0.712	1.750	80142.	167915.
4	6.0	.750	0.	474.	354.	.0020	82000.	0.857	1.750	92793.	167915.
4	6.0	.750	0.	474.	354.	.0024	73800.	0.992	1.750	103270.	167915.
4	6.0	.750	0.	474.	354.	.0028	69700.	1.117	1.750	112225.	167915.
4	6.0	.750	0.	474.	354.	.0032	65600.	1.232	1.750	120057.	167915.
4	6.0	.750	0.	474.	354.	.0036	57400.	1.340	1.750	126662.	167915.
4	6.0	.750	0.	474.	354.	.0040	53300.	1.440	1.750	132187.	167915.
4	6.0	.750	0.	474.	354.	.0044	51250.	1.532	1.750	137041.	167915.
4	6.0	.750	0.	474.	354.	.0048	51250.	1.619	1.750	141456.	167915.
4	6.0	.750	0.	474.	354.	.0052	49200.	1.698	1.750	145452.	167915.
4	6.0	.750	0.	474.	354.	.0056	47150.	1.771	1.750	148977.	167915.
4	6.0	.750	0.	474.	354.	.0060	49200.	1.838	1.750	152202.	167915.
4	6.0	.750	0.	474.	354.	.0064	47150.	1.899	1.750	155126.	167915.
4	6.0	.750	0.	474.	354.	.0068	47150.	1.954	1.750	157697.	167915.
4	6.0	.750	0.	474.	354.	.0072	45100.	2.002	1.750	159933.	167915.
4	6.0	.750	0.	474.	354.	.0076	41000.	2.045	1.750	161771.	167915.
4	6.0	.750	0.	474.	354.	.0080	38950.	2.082	1.750	163263.	167915.
4	6.0	.750	0.	474.	354.	.0084	32800.	2.114	1.750	164425.	167915.
4	6.0	.750	0.	474.	354.	.0088	28700.	2.142	1.750	165288.	167915.
4	6.0	.750	0.	474.	354.	.0092	26650.	2.167	1.750	165961.	167915.
4	6.0	.750	0.	474.	354.	.0096	22550.	2.188	1.750	166475.	167915.
4	6.0	.750	0.	474.	354.	.0100	16400.	2.206	1.750	166827.	167915.
4	6.0	.750	0.	474.	354.	.0104	10250.	2.222	1.750	167039.	167915.
4	6.0	.750	0.	474.	354.	.0108	6150.	2.236	1.750	167158.	167915.
4	6.0	.750	0.	474.	354.	.0112	4100.	2.250	1.750	167228.	167915.
4	6.0	.750	0.	474.	354.	.0116	4100.	2.263	1.750	167281.	167915.
4	6.0	.750	0.	474.	354.	.0120	2050.	2.276	1.750	167320.	167915.
4	6.0	.750	0.	474.	354.	.0124	0.	2.288	1.750	167333.	167915.

I	HT (IN)	THK (IN)	ANG (DEG)	WT (LB)	ELE (IN)	TIME (SEC)	FORCE (LB)	DEF (IN)	MEAS (IN)	CAL U (IN-LB)	U IN (IN-LB)
5	9.0	.750	0.	474.	351.	.0	135300.	0.0	6.000	0.	166493.
5	9.0	.750	0.	474.	351.	.0010	82000.	0.475	6.000	51649.	166493.
5	9.0	.750	0.	474.	351.	.0020	22550.	0.886	6.000	73092.	166493.
5	9.0	.750	0.	474.	351.	.0030	16400.	1.267	6.000	80514.	166493.
5	9.0	.750	0.	474.	351.	.0040	14350.	1.634	6.000	86157.	166493.
5	9.0	.750	0.	474.	351.	.0050	14350.	1.989	6.000	91251.	166493.
5	9.0	.750	0.	474.	351.	.0060	12300.	2.332	6.000	95831.	166493.
5	9.0	.750	0.	474.	351.	.0070	10250.	2.666	6.000	99595.	166493.
5	9.0	.750	0.	474.	351.	.0080	8200.	2.992	6.000	102598.	166493.
5	9.0	.750	0.	474.	351.	.0090	8200.	3.310	6.000	105209.	166493.
5	9.0	.750	0.	474.	351.	.0100	14350.	3.621	6.000	108710.	166493.
5	9.0	.750	0.	474.	351.	.0110	18450.	3.920	6.000	113619.	166493.
5	9.0	.750	0.	474.	351.	.0120	14350.	4.206	6.000	118310.	166493.
5	9.0	.750	0.	474.	351.	.0130	10250.	4.480	6.000	121686.	166493.
5	9.0	.750	0.	474.	351.	.0140	20500.	4.744	6.000	125732.	166493.
5	9.0	.750	0.	474.	351.	.0150	16400.	4.993	6.000	130336.	166493.
5	9.0	.750	0.	474.	351.	.0160	16400.	5.229	6.000	134196.	166493.
5	9.0	.750	0.	474.	351.	.0170	14350.	5.451	6.000	137618.	166493.
5	9.0	.750	0.	474.	351.	.0180	14350.	5.662	6.000	140638.	166493.
5	9.0	.750	0.	474.	351.	.0190	12300.	5.861	6.000	143293.	166493.
5	9.0	.750	0.	474.	351.	.0230	12300.	6.557	6.000	151852.	166493.
5	9.0	.750	0.	474.	351.	.0240	14350.	6.705	6.000	153832.	166493.
5	9.0	.750	0.	474.	351.	.0250	12300.	6.843	6.000	155668.	166493.
5	9.0	.750	0.	474.	351.	.0260	14350.	6.970	6.000	157361.	166493.
5	9.0	.750	0.	474.	351.	.0270	12300.	7.086	6.000	158910.	166493.
5	9.0	.750	0.	474.	351.	.0280	10250.	7.193	6.000	160108.	166493.
5	9.0	.750	0.	474.	351.	.0290	8200.	7.291	6.000	161012.	166493.
5	9.0	.750	0.	474.	351.	.0300	6150.	7.382	6.000	161667.	166493.
5	9.0	.750	0.	474.	351.	.0310	6150.	7.468	6.000	162196.	166493.
5	9.0	.750	0.	474.	351.	.0320	4100.	7.549	6.000	162612.	166493.
5	9.0	.750	0.	474.	351.	.0330	2050.	7.627	6.000	162852.	166493.
5	9.0	.750	0.	474.	351.	.0340	0.	7.704	6.000	162931.	166493.

I	HT (IN)	THK (IN)	ANG (DEG)	WT (LB)	ELE (IN)	TIME (SEC)	FORCE (LB)	DEF (IN)	MEAS (IN)	CAL U (IN-LB)	U IN (IN-LB)
6	9.0	.750	0.	304.	351.	.0	133250.	0.0	1.750	0.	106780.
6	9.0	.750	0.	304.	351.	.0010	71750.	0.455	1.750	46601.	106780.
6	9.0	.750	0.	304.	351.	.0020	45100.	0.808	1.750	67226.	106780.
6	9.0	.750	0.	304.	351.	.0030	30750.	1.100	1.750	78306.	106780.
6	9.0	.750	0.	304.	351.	.0040	26650.	1.350	1.750	85483.	106780.
6	9.0	.750	0.	304.	351.	.0050	22550.	1.566	1.750	90807.	106780.
6	9.0	.750	0.	304.	351.	.0060	21525.	1.753	1.750	94927.	106780.
6	9.0	.750	0.	304.	351.	.0070	20500.	1.913	1.750	98284.	106780.
6	9.0	.750	0.	304.	351.	.0080	19475.	2.047	1.750	100960.	106780.
6	9.0	.750	0.	304.	351.	.0090	18450.	2.156	1.750	103032.	106780.
6	9.0	.750	0.	304.	351.	.0100	12300.	2.244	1.750	104379.	106780.
6	9.0	.750	0.	304.	351.	.0110	2050.	2.317	1.750	104905.	106780.
6	9.0	.750	0.	304.	351.	.0120	0.	2.385	1.750	104975.	106780.

I	HT (IN)	THK (IN)	ANG (DEG)	WT (LB)	ELE (IN)	TIME (SEC)	FORCE (LB)	DEF (IN)	MEAS (IN)	CAL U (IN-LB)	U IN (IN-LB)
7	8.0	.500	0.	178.	352.	.C	0.	0.0	3.437	C.	62656.
7	8.0	.500	0.	178.	352.	.0010	30750.	0.503	3.437	7739.	62656.
7	8.0	.500	0.	178.	352.	.0020	18025.	0.964	3.437	18969.	62656.
7	8.0	.500	0.	178.	352.	.0030	14750.	1.380	3.437	25794.	62656.
7	8.0	.500	0.	178.	352.	.0040	12300.	1.765	3.437	30990.	62656.
7	8.0	.500	0.	178.	352.	.0050	14750.	2.120	3.437	35792.	62656.
7	8.0	.500	0.	178.	352.	.0060	11475.	2.446	3.437	40071.	62656.
7	8.0	.500	0.	178.	352.	.0070	10650.	2.746	3.437	43392.	62656.
7	8.0	.500	0.	178.	352.	.0080	8200.	3.024	3.437	46014.	62656.
7	8.0	.500	0.	178.	352.	.0090	6970.	3.284	3.437	47984.	62656.
7	8.0	.500	0.	178.	352.	.0100	6150.	3.529	3.437	49588.	62656.
7	8.0	.500	0.	178.	352.	.0110	6970.	3.759	3.437	51099.	62656.
7	8.0	.500	0.	178.	352.	.0120	13500.	3.971	3.437	53272.	62656.
7	8.0	.500	0.	178.	352.	.0130	15575.	4.157	3.437	55969.	62656.
7	8.0	.500	0.	178.	352.	.0140	14350.	4.310	3.437	58269.	62656.
7	8.0	.500	0.	178.	352.	.0150	12300.	4.434	3.437	59911.	62656.
7	8.0	.500	0.	178.	352.	.0160	12700.	4.529	3.437	61103.	62656.
7	8.0	.500	0.	178.	352.	.0170	13500.	4.597	3.437	61990.	62656.
7	8.0	.500	0.	178.	352.	.0180	13100.	4.636	3.437	62512.	62656.

I	HT (IN)	THK (IN)	ANG (DEG)	WT (LB)	ELE (IN)	TIME (SEC)	FORCE (LB)	DEF (IN)	MEAS (IN)	CAL U (IN-LB)	U IN (IN-LB)
8	8.0	.500	0.	157.	352.	.0	30750.	0.0	2.250	0.	55264.
8	8.0	.500	0.	157.	352.	.0010	30750.	0.482	2.250	14832.	55264.
8	8.0	.500	0.	157.	352.	.0020	22950.	0.894	2.250	25891.	55264.
8	8.0	.500	0.	157.	352.	.0030	19675.	1.247	2.250	33414.	55264.
8	8.0	.500	0.	157.	352.	.0040	18025.	1.551	2.250	39142.	55264.
8	8.0	.500	0.	157.	352.	.0050	15175.	1.812	2.250	43467.	55264.
8	8.0	.500	0.	157.	352.	.0060	14350.	2.034	2.250	46747.	55264.
8	8.0	.500	0.	157.	352.	.0070	12700.	2.221	2.250	49284.	55264.
8	8.0	.500	0.	157.	352.	.0080	10650.	2.378	2.250	51114.	55264.
8	8.0	.500	0.	157.	352.	.0090	8720.	2.509	2.250	52379.	55264.
8	8.0	.500	0.	157.	352.	.0100	4510.	2.619	2.250	53111.	55264.
8	8.0	.500	0.	157.	352.	.0110	9020.	2.714	2.250	53750.	55264.
8	8.0	.500	0.	157.	352.	.0120	4920.	2.791	2.250	54290.	55264.
8	8.0	.500	0.	157.	352.	.0130	9850.	2.851	2.250	54733.	55264.
8	8.0	.500	0.	157.	352.	.0140	8200.	2.891	2.250	55093.	55264.
8	8.0	.500	0.	157.	352.	.0150	6660.	2.911	2.250	55241.	55264.

I	HT (IN)	THK (IN)	ANG (DEG)	WT (LB)	ELE (IN)	TIME (SEC)	FORCE (LB)	DEF (IN)	MEAS (IN)	CAL U (IN-LB)	U IN (IN-LB)
9	6.0	.500	0.	157.	354.	.0	76950.	0.0	1.250	0.	55578.
9	6.0	.500	0.	157.	354.	.0010	55400.	0.440	1.250	29149.	55578.
9	6.0	.500	0.	157.	354.	.0020	35900.	0.744	1.250	43015.	55578.
9	6.0	.500	0.	157.	354.	.0030	25650.	0.954	1.250	49486.	55578.
9	6.0	.500	0.	157.	354.	.0040	23600.	1.097	1.250	52995.	55578.
9	6.0	.500	0.	157.	354.	.0050	21550.	1.182	1.250	54909.	55578.
9	6.0	.500	0.	157.	354.	.0060	18450.	1.215	1.250	55564.	55578.

I	HT (IN)	THK (IN)	ANG (DEG)	WT (LB)	ELE (IN)	TIME (SEC)	FORCE (LB)	DEF (IN)	MEAS (IN)	CAL U (IN-LB)	U IN (IN-LB)
10	6.0	.500	0.	157.	354.	.0	66660.	0.0	1.000	0.	55578.
10	6.0	.500	0.	157.	354.	.0004	86200.	0.194	1.000	14798.	55578.
10	6.0	.500	0.	157.	354.	.0008	66660.	0.357	1.000	27309.	55578.
10	6.0	.500	0.	157.	354.	.0012	63600.	0.493	1.000	36167.	55578.
10	6.0	.500	0.	157.	354.	.0016	48200.	0.606	1.000	42446.	55578.
10	6.0	.500	0.	157.	354.	.0020	31800.	0.699	1.000	46188.	55578.
10	6.0	.500	0.	157.	354.	.0024	28700.	0.779	1.000	48602.	55578.
10	6.0	.500	0.	157.	354.	.0028	27700.	0.847	1.000	50530.	55578.
10	6.0	.500	0.	157.	354.	.0032	26660.	0.905	1.000	52094.	55578.
10	6.0	.500	0.	157.	354.	.0036	23600.	0.952	1.000	53283.	55578.
10	6.0	.500	0.	157.	354.	.0040	22570.	0.990	1.000	54157.	55578.

APPENDIX C

EXAMPLE PROBLEM

An example problem is presented here to demonstrate the intended use of the results of this investigation in the analysis of cylindrical shipping casks for radioactive materials that have external longitudinal fins with respect to the 30-foot free-drop hypothetical accident condition. The curves shown in Figures 5.1 through 5.5 (pages 29 through 33) may be used to determine the energy absorption capability of the longitudinal fins along the cask body, and the curves shown in Figures 5.10 through 5.14 (pages 42 through 46) may be used to determine the peak force to which these fins would be subjected during their collapse resulting from the 30-foot free drop and impact of the cask upon an essentially unyielding horizontal surface.

The cylindrical shipping cask of this example problem has mild-steel fins along its longitudinal axis that are 8 inches high (measured from the outer surface of the cask to the fin tip) and 1/2 inch thick. The length of each fin along the cask body is 60 inches. The cask will free fall through a vertical distance of 30 feet to impact an essentially unyielding horizontal surface on its side. The circumferential spacing of the fins around the cask body is such that upon initial impact, two fins will strike the horizontal surface at a 10-degree angle of inclination and deform 45 percent and two other fins will strike the surface at a 30-degree angle and deform 15 percent before the cask body contacts the essentially unyielding horizontal surface.

The static plastic moment of each of these fins is determined from the expression

$$M_p = \sigma_y\left(\frac{bt^2}{4}\right) , \tag{5.1}$$

where

σ_y = yield stress of fin material = 30,000 pounds per square inch,

b = length of fin = 60 inches, and

t = thickness of fin = 1/2 inch.

$$M_p = 112{,}500 \text{ inch-pounds} .$$

Figure 5.2 (page 30) is used and the curve for specimens with a height H = 8 inches is selected to determine the value of the absorbed energy divided by the static plastic moment for specimens impacted with a 10-degree angle of inclination. At a deformation of 45 percent, this value for 8-inch-high specimens is read as 16. The value of 16 multiplied by the static plastic moment value of 112,500 inch-pounds calculated by using Equation 5.1 gives the amount of energy that would be absorbed by one fin striking the horizontal surface at a 10-degree angle of inclination and deforming 45 percent. This energy is 1,800,000 inch-pounds.

Figure 5.4 (page 32) is used and the curve for specimens with a height H = 8 inches is selected to determine the value of absorbed energy divided by the static plastic moment for specimens impacted with a 30-degree angle of inclination. At a deformation of 15 percent, this value for 8-inch-high specimens is read as 1.1. The value of 1.1 multiplied by the static plastic moment value of 112,500 inch-pounds that was calculated by using Equation 5.1 gives approximately 124,000 inch-pounds

of energy absorbed by one cask fin impacting the horizontal surface at a 30-degree angle of inclination and deforming 15 percent.

The total energy absorbed by the cask fins of this example problem during the impact resulting from the 30-foot free drop onto an essentially unyielding horizontal surface would be

$$2(1,800,000) + 2(124,000) = 3,850,000 \text{ inch-pounds} .$$

The peak force experienced by the shipping cask of this example problem would occur shortly after the initial impact of the two fins striking the horizontal surface at a 10-degree angle of inclination. The height-to-thickness ratio of the cask fins in this problem is 16, and the peak force expected to be experienced by the fins impacting at a 10-degree angle of inclination is read from the curve in Figure 5.11 (page 43) as approximately 37,500 pounds per linear inch of fin. When this value is multiplied by the fin length (60 inches) and the result is doubled to account for both the fins impacting at a 10-degree angle, the resulting peak force value is 4,500,000 pounds. The peak force the cask would experience as a result of the collapse of the two fins impacting the horizontal surface at a 30-degree angle of inclination would occur later in the impact event and be of much less magnitude and significance.

Internal Distribution

1. M. Bender
2. C. E. Bettis
3. D. D. Cannon
4. F. L. Culler, Jr.
5-8. F. C. Davis
9. H. G. Duggan
10. J. H. Evans
11. W. F. Ferguson
12. F. C. Fitzpatrick
13. W. R. Gall
14. J. H. Gillette
15. K. W. Haff
16. A. R. Irvine
17. E. M. King
18. B. B. Klima
19. R. J. Lauer
20. A. J. Mallett (K-25)
21. J. R. McGuffey
22. J. D. McLendon (Y-12)
23. H. A. Nelms
24. T. W. Pickel, Jr.
25. A. F. Rupp
26. R. D. Seagren
27-31. L. B. Shappert
32. W. C. T. Stoddart
33. J. Thomas (Y-12)
34. W. E. Unger
35. H. K. Walker
36. D. C. Watkin
37. W. R. Winsbro
38-39. Central Research Library
40. Document Reference Section
41. GE Division Library
42-54. Laboratory Records Department
55. Laboratory Records, ORNL R.C.
56. ORNL Patent Office

External Distribution

57. F. E. Adcock, The Dow Chemical Company, Rocky Flats Division, Post Office Box 888, Golden, Colorado 80401
58. W. L. Albrecht, Tennessee Valley Authority, New Sprankle Building, Knoxville, Tennessee 37902
59. A. Anselmo, Idaho Nuclear Corporation, Post Office Box 1845, Idaho Falls, Idaho 83401
60. R. F. Barker, USAEC, Division of Radiation Protection, Washington, D. C. 20545
61. R. J. Bass, E. I. du Pont de Nemours & Company, Savannah River Plant, Aiken, South Carolina 29801
62. W. G. Belter, USAEC, Division of Reactor Development and Technology, Washington, D. C. 20545

63. W. A. Brobst, USAEC, Division of Construction, Washington, D. C. 20545

64. C. L. Brown, Pacific Northwest Laboratory, Richland, Washington 99352

65. C. W. Buckland, Los Alamos Scientific Laboratory, Post Office Box 1663, Los Alamos, New Mexico 87544

66. F. J. Bush, Jr., National Lead Company, Foot of West Street, Wilmington, Delaware 19898

67. C. M. Copenhaver, USAEC, Oak Ridge Operations Office, Post Office Box E, Oak Ridge, Tennessee 37830

68. B. D. Devine, Argonne National Laboratory, 9700 South Cass Avenue, Argonne, Illinois 60439

69. D. L. Dunaway, National Lead Company of Ohio, Post Office Box 39158, Cincinnati, Ohio 45239

70. D. A. Edling, Mound Laboratory, Monsanto Research Corporation, Miamisburg, Ohio 45342

71. C. S. Ehrman, Allied Chemical Corporation, Post Office Box 35, Florham Park, New Jersey 07932

72. J. T. Foley, Sandia Laboratories, Post Office Box 5800, Albuquerque, New Mexico 87115

73. W. P. Gammill, USAEC, Division of Reactor Development and Technology, Washington, D. C. 20545

74. C. Glidewell, Tennessee Valley Authority, 200 Arnstein Building, Knoxville, Tennessee 37902

75. A. W. Grella, U. S. Department of Transportation, 6th and D Street SW, Washington, D. C. 20590

76. D. A. Hoover, Atlantic Richfield Hanford Company, Richland, Washington 99352

77. L. H. Horn, Underwriters' Laboratories, 207 E. Ohio Street, Chicago, Illinois 60611

78. W. R. Householder, HGS Technical Associates, Inc., Post Office Box 1156, Johnson City, Tennessee 37601

79. P. C. Huang, Bureau of Naval Ordnance Laboratory, Silver Spring, Maryland 20907

80. R. I. Jetter, Atomics International, Post Office Box 309, Canoga Park, California 91304

81. J. W. Jones, Bettis Atomic Power Laboratory, Post Office Box 79, West Mifflin, Pennsylvania 15122

82. B. A. Karrasch, The Babcock & Wilcox Company, Post Office Box 1260, Lynchburg, Virginia 24505

83. R. E. Kropp, United Nuclear Corporation, Post Office Box 1883, New Haven, Connecticut 06508

84. W. Legler, Allied Chemical, In care of Bectel Corporation, 50 Beale Street, San Francisco, California 94105

85. J. W. Langhaar, E. I. du Pont de Nemours & Company, Wilmington, Delaware, 19898

86. R. E. Lipenski, USAEC, Division of Materials Licensing, Washington, D. C. 20545

87. E. C. Lusk, Battelle Memorial Institute, 505 King Avenue Avenue, Columbus, Ohio 43201

88. W. C. McCluggage, USAEC, Division of Operational Safety, Washington, D. C. 20545

89. J. S. Milau, Brookhaven National Laboratory, Upton, L. I., New York 11973

90. W. A. Nelson, USAEC, Division of Reactor Development and Technology, Washington, C. C. 20545

91. H. E. Noyes, Los Alamos Scientific Laboratory, Post Office Box 1663, Los Alamos, New Mexico 87544

92. R. H. Odegaarden, USAEC, Division of Materials Licensing, Washington, D. C. 20545

93. R. W. Peterson, Allied Chemical Corporation, Post Office Box 35, Florham Park, New Jersey 07932

94. H. Pih, Department of Engineering Mechanics, The University of Tennessee, Knoxville, Tennessee 37916

95. W. A. Pryor, USAEC, Oak Ridge Operations Office, Post Office Box E, Oak Ridge, Tennessee 37830

96. S. L. Reese, Nuclear Safety Associates, Suite 200, 7735 Old Georgetown Road, Bethesda, Maryland 20014

97. R. F. Rogers, E. I. du Pont de Nemours & Company, Savannah River Plant, Aiken, South Carolina 29801

98. L. Rutland, Atcor, Inc., No. 5 West Chester Plaza, Elmsford, New York 10523

99. H. P. Shaw, Atlantic Richfield Hanford Company, Post Office Box 250, Richland, Washington 99352

100. L. R. Shobe, Department of Engineering Mechanics, The University of Tennessee, Knoxville, Tennessee 37916

101. J. A. Sisler, USAEC, Traffic Management Branch, Washington, D. C. 20545

102. C. W. Smith, General Electric Company, 283 Brokaw Road, Santa Clara, California 95050

103. D. R. Smith, Los Alamos Scientific Laboratory, Post Office Box 1663, Los Alamos, New Mexico 87544

104. D. R. Swindle, USAEC, Division of Construction, Washington, D. C. 20545

105. R. J. Thompson, Stearns-Roger Corporation, Post Office Box 5888, Denver, Colorado 80217

106. H. E. Walchli, Westinghouse Electric Corporation, Post Office Box 355, Pittsburgh, Pennsylvania 15230

107. R. B. Waite, Stearns-Roger Corporation, Post Office Box 5888, Denver, Colorado 80217

108-122. Division of Technical Information Extension, USAEC

123. Laboratory and University Division, USAEC, ORO